Marine and Petroleum Geology 123 (2021) 104770

Contents lists available at ScienceDirect

Marine and Petroleum Geology

journal homepage: www.elsevier.com/locate/marpetgeo

Research paper

Salt tectonics and controls on halokinetic-sequence development of an exposed deepwater diapir: The Bakio Diapir, Basque-Cantabrian Basin, Pyrenees

Eduard Roca [a,*], Oriol Ferrer [a], Mark G. Rowan [b], Josep Anton Muñoz [a], Mireia Butillé [a], Katherine A. Giles [c], Pau Arbués [a], Marco de Matteis [a]

[a] Institut de Recerca GEOMODELS, Departament de Dinàmica de la Terra i de l'Oceà, Universitat de Barcelona (UB), Barcelona, Spain
[b] Rowan Consulting, Inc., Boulder, CO, USA
[c] Institute of Tectonic Studies, Department of Geological Sciences, University of Texas at El Paso, El Paso, TX, USA

ARTICLE INFO

Keywords:
Salt tectonics
Deepwater sediments
Carbonate and turbidite systems
Salt diapirs
Salt-sediment interaction
Basque-Cantabrian Basin

ABSTRACT

This work evaluates growth strata adjacent to the Bakio Diapir in the Basque Pyrenees, aiming to discuss the application of halokinetic-sequence concepts, mainly developed in shallow-water to subaerial environments, to deepwater depositional settings. This is one of the few exposed passive diapirs developed in deepwater environments, with both synkinematic carbonate and siliciclastic strata. Thus, considering that large hydrocarbon producing areas are located in salt provinces developed in deepwater environments, this study is of interest not only to researchers in salt tectonics, but also to industry geoscientists focusing on hydrocarbon exploration and production. We present a 3D analysis of this outstanding salt structure by integrating detailed geological cartography, high-resolution bathymetry, seismic, and well data. The resulting reconstruction enables us to trace the extent of the diapir offshore and decipher its evolution from its formation as a salt wall developed above the overlap of two basement-involved faults until its squeezing during the Pyrenean compression. But more significantly, it allows us to discern the roles played by bathymetry, subsidence, and sedimentation type in the configuration of halokinetic sequences developed in deepwater environments. Thus, our study shows that: 1) the geometry of halokinetic sequences is defined by the thickness of the roof edges, the dip of the salt-sediment interface in the limbs of the active drape fold, and the onlap angle of the synkinematic sediments over the salt; 2) the roof thickness is controlled not only by the ratio between salt-rise and regional sediment-accumulation rate, but also by the water depth of the diapir roof and the depositional environment that can promote vertical aggradation of a supra-diapir carbonate buildup; and 3) high surface slopes and consequent debrites are not exclusive to, and characteristic of, hook halokinetic sequences and tabular composite halokinetic sequences.

1. Introduction

Many of the world's great hydrocarbon provinces are hosted in sedimentary basins involving salt (e.g., Gulf of Mexico, Campos Basin, Persian Gulf, North Sea), which have been affected by salt-related deformation that creates structures and traps, influences reservoir distribution, and controls hydrocarbon migration (e.g., Warren, 2006; Hudec and Jackson, 2007; Jackson and Hudec, 2017). Hence, understanding the geometry and kinematics of salt structures has become fundamental for effective hydrocarbon exploration in many sedimentary basins. The geometry of structures can be observed at the surface or imaged in the subsurface by geophysical data, but deciphering their kinematics requires detailed studies of the tectono-sedimentary relationships. Detailed analysis of growth strata has proved a powerful methodology to unravel the kinematic evolution of structures in any tectonic setting, including salt tectonics (Poblet et al., 1998; Prather et al., 1998; Hudec et al., 2009; Giles and Rowan, 2012; Alsop et al., 2016).

* Corresponding author. Institut de Recerca GEOMODELS, Departament de Dinàmica de la Terra i de l'Oceà, Universitat de Barcelona (UB), c/ Martí i Franquès s/n, 08028, Barcelona, Spain.
E-mail address: eduardroca@ub.edu (E. Roca).

https://doi.org/10.1016/j.marpetgeo.2020.104770
Received 17 April 2020; Received in revised form 23 September 2020; Accepted 15 October 2020
Available online 16 October 2020

In the case of passive diapirs, the fundamental features for understanding the kinematics are the geometry of the salt-sediment interface as well as the architecture and facies of flanking synkinematic strata. These are characterized by packages of growth strata bounded by unconformities that become conformable away from salt bodies and merge with the diapirs at small cusps in the salt-sediment interface (Giles and Lawton, 2002; Rowan et al., 2003). Defined by Giles and Lawton (2002), these stratal packages have been termed halokinetic sequences and form by drape folding of the diapir roof during passive salt rise (Rowan et al., 2003). They show different features that depend on the ratio of salt-rise and sediment-accumulation rates (Giles and Rowan, 2012; Hearon et al., 2014) (Fig. 1). Thus, if the salt-rise rate exceeds the sediment-accumulation rate, the synkinematic strata are characterized by tabular composite halokinetic sequences (CHS) formed by hook halokinetic sequences (HS) that are bounded by high-angle unconformities extending over a distance of 20–200 m from the diapir edge (Fig. 1A). In contrast, if sedimentation rate exceeds salt-rise rate, sedimentary packages form wedge HS in which the bounding unconformities extend farther (300–1000 m) from the diapir and have lower angularity, thereby defining tapered CHS (Fig. 1B). Note that the capping unconformity of a tapered CHS can be high-angle (Fig. 1B, bottom), giving it the appearance of a large-scale hook (Giles and Rowan, 2012).

This classification was mostly derived from direct observations of outcrops in La Popa Basin, Mexico, and the Flinders Ranges, South Australia (Giles and Lawton, 2002; Rowan et al., 2003, 2012a; Kernen et al., 2012; Hearon et al., 2015; Counts et al., 2019), where the halokinetic sequences contain mostly siliciclastic or mixed sediments deposited in shallow-water to subaerial depositional environments. The concepts have been successfully applied in other salt provinces with similar depositional environments (e.g., the Atlas Mts. of Morocco, the Pyrenees of Spain and France, or the Sivas Basin of Turkey) (Ringenbach et al., 2013; Saura et al., 2014, 2016; Ribes et al., 2015; Kergaravat et al., 2017).

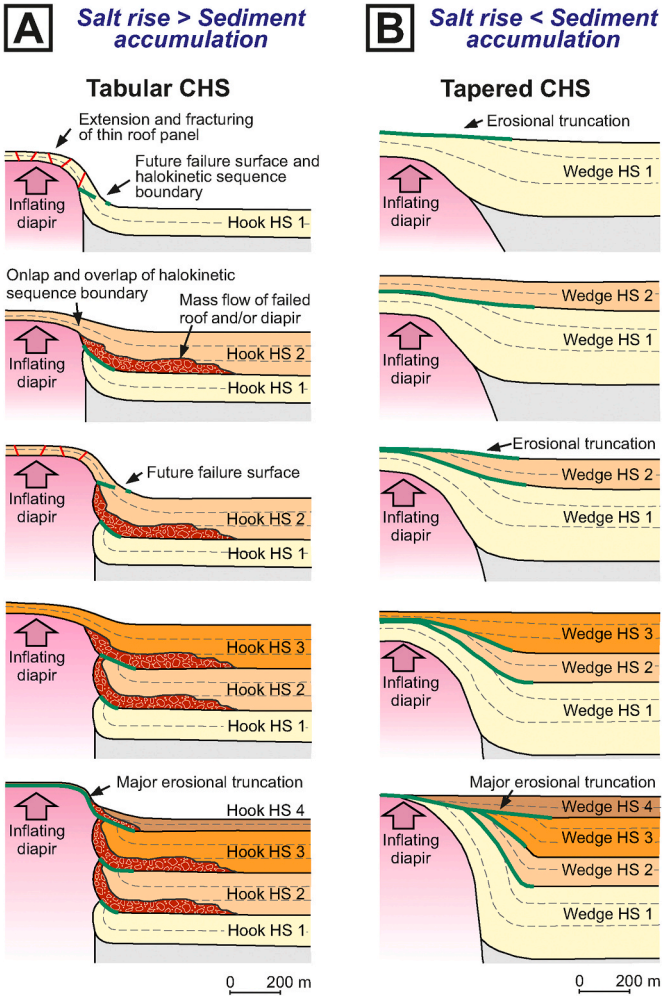

Fig. 1. Types of composite halokinetic sequences (CHS) defined in shallow to subaerial environments and their corresponding genetic models (modified from Giles and Rowan, 2012). **A)** Hook halokinetic sequences (HS) stacked into a tabular CHS; **B)** Wedge HS stacked into a tapered CHS.

In deepwater depositional environments like the Gulf of Mexico or Campos Basin, however, the applicability of this model is not so clear. Present-day seafloor images (Ryan et al., 2009) and seismic reflection profiles (Rowan et al., 2003; Hearon et al., 2014; Coleman et al., 2018) show similar halokinetic sequences with geometries and seismic facies that are mostly compatible with the proposed halokinetic sequence model (Hearon et al., 2014). But the lack of well-studied outcrop analogs still generates certain doubts about the direct applicability of this model. Indeed, exposed diapirs containing deepwater halokinetic sequences are rare and usually poorly exposed due either to weathering or cover by dense vegetation (e.g. Alps, Carpathians, or Pyrenees).

In this sense, the Bakio Diapir appears to be one of the few opportunities to analyze at the surface a diapir developed in a deepwater depositional environment. Located in the Basque Pyrenees (Fig. 2), this diapir is flanked by carbonate outer-shelf to siliciclastic deepwater strata (García-Mondejar and Robador, 1987; Robador and García-Mondejar, 1987; Robles et al., 1988). It has been recognized that these strata form composite halokinetic sequences (Rowan et al., 2012b; Ferrer et al., 2014; Poprawski et al., 2014; Cumberpatch et al., 2020), with growth of a carbonate platform above the diapir in relative deepwater conditions resulting in the formation of wedge HS/tapered CHS with abundant and thick debrites (Rowan et al., 2012b; Poprawski et al., 2016). These features contrast with the established model, in which wedge HS/tapered CHS are characterized by a relative lack of debrites (Giles and Rowan, 2012).

The published studies dealing with this diapir have been based only on analyses of data collected in the field or by airborne LIDAR along a narrow coastline strip that crosses the best outcrops of the diapir and related halokinetic sucessions. Moreover, they have focused on the older halokinetic sequences that are formed primarily by carbonate sediments (Rowan et al., 2012b; Poprawski et al., 2014, 2016). Thus, they have not evaluated the 3D geometry of the diapir, the possible lateral variations of the halokinetic sequences, or the detailed architecture of the upper halokinetic sequences that comprise exclusively siliciclastic gravity-flow deposits. Moreover, they have not addressed the geodynamic context in which the diapir grew and the impact that this could have had on its development.

In this framework, our study aims to fill these gaps through the reconstruction of the 3D geometry of the Bakio Diapir and surrounding halokinetic sequences utilizing information provided by the available seismic reflection profiles, the near-shore seafloor bathymetry, and detailed geological mapping of both the coastline and forested inland areas. This reconstruction allows us to: 1) decipher the formation and evolution of the diapir; 2) analyze the roles played by bathymetry, subsidence history, and sedimentation type in the configuration of the halokinetic sequences developed in outer-shelf, slope, and deepwater environments; and 3) at a larger scale, evaluate the impact on the diapir evolution of changes in rift style during the development of the Basque-Cantabrian Basin. Accordingly, and considering that large hydrocarbon producing areas are located in salt provinces developed in deepwater environments and extensional tectonic scenarios (e.g., Gulf of Mexico or South Atlantic passive margins), the results should be useful not only to researchers in salt tectonics, but also to industry geoscientists whose efforts are focused on hydrocarbon exploration and production.

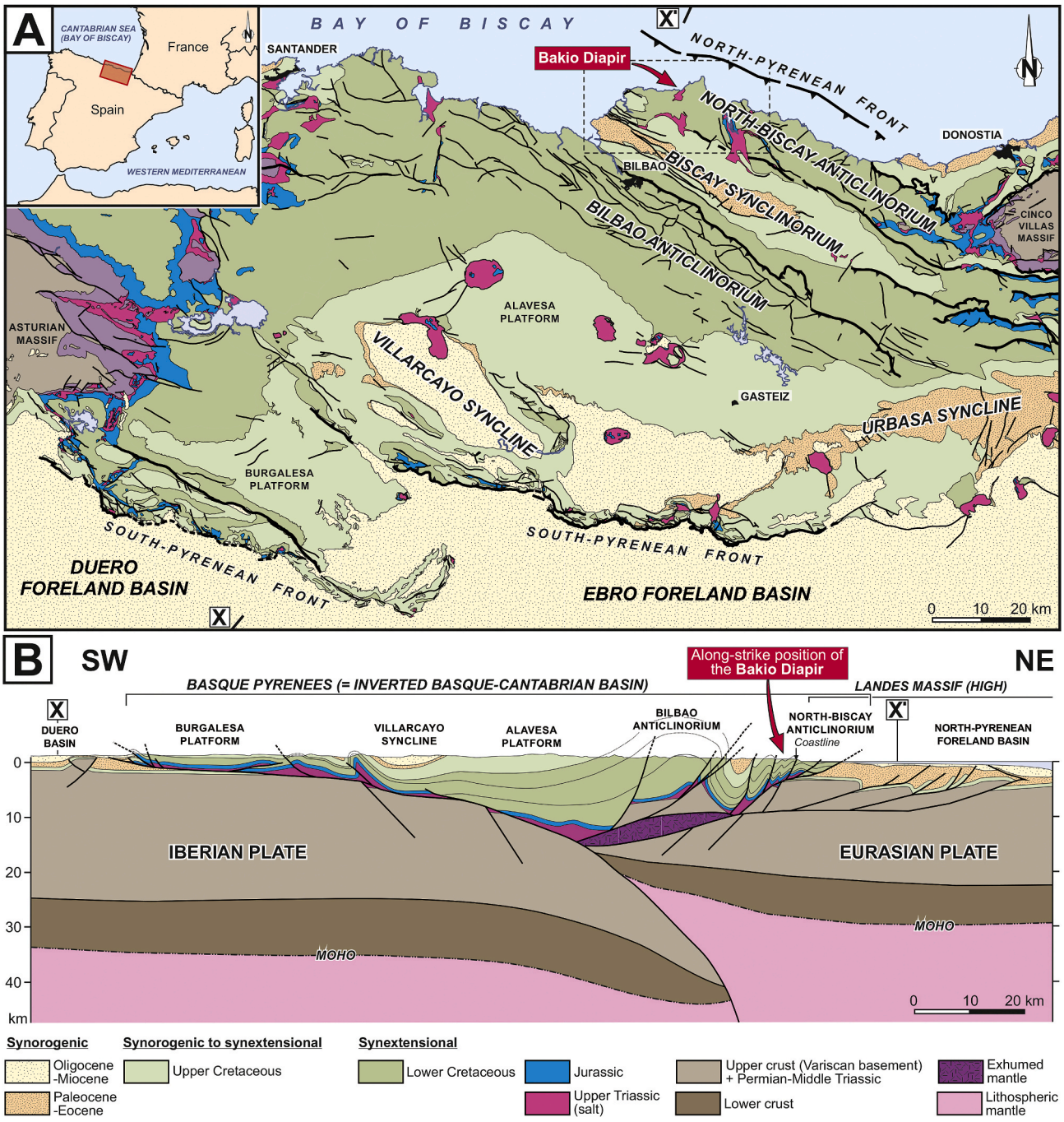

Fig. 2. A) Location and geologic map of the Basque Pyrenees, which formed by tectonic inversion of the Upper Jurassic-Lower Cretaceous hyperextended Basque-Cantabrian Basin. Note the location of the studied Bakio Diapir at the northern edge of this inverted basin. X-X': location of the transect shown in Fig. 2B. Dashed rectangle: location of the geologic map of Fig. 3. **B)** Crustal cross section through the Basque Pyrenees illustrating the main features of the inverted Basque-Cantabrian Basin and associated salt structures concentrated at the basin margins (modified from Quintana et al., 2015; Carola et al., 2015). See location in Fig. 2A (X-X').

2. Geological setting of the Basque-Cantabrian Basin

2.1. Overview

The Bakio Diapir is a salt diapir located at the northern margin of the Basque-Cantabrian Basin (Fig. 2A). This basin developed between the Iberian and Eurasian plates during the latest Jurassic-Cretaceous opening of the Bay of Biscay (Sibuet et al., 2004; Tugend et al., 2014) and was later inverted during the Pyrenean orogeny (Late Cretaceous -Santonian- to middle Miocene; Muñoz, 2002), forming the Basque Pyrenees. The Basque-Cantabrian Basin is a 250 km long and 100 km wide hyperextended basin (Roca et al., 2011) that, in its central parts, was floored by an extremely thinned lithosphere with exhumed mantle (Mendia and Gil-Ibarguchi, 1991; DeFelipe et al., 2017; Pedrera et al., 2017).

In accordance with this extreme thinning, the infill of the Basque-Cantabrian Basin is very thick, with up to 12.5 km of synrift to postrift Upper Jurassic-Cretaceous shallow- to deepwater marine sediments (Floquet, 2004; García-Mondéjar et al., 2004). The underlying Mesozoic prerift strata comprise relatively thin (hundreds of meters thick) Lower-Middle Jurassic carbonates overlying Upper Triassic evaporites. These evaporites (Keuper facies) were deposited during the late stages of

Permo-Triassic rifting (López-Gómez et al., 2019) and their distribution controlled the morphology and deformation style of the subsequent Late Jurassic-Early Cretaceous extensional basins. In particular, in areas where the evaporites were thick enough, they sourced diapiric structures and decoupled both extensional and contractional deformation, acting as a major décollement (Fig. 2B).

Thus, the Jurassic-Cenozoic rocks of the Basque Pyrenees, partly detached from basement by the Upper Triassic salt, form an asymmetric double-wedge (Ferrer et al., 2008; Muñoz, 2019) with: 1) a wider, southern pro-wedge floored by a major south-directed thrust that transported a gently deformed suprasalt cover (Martínez-Torres, 1993; Quintana, 2012; Carola et al., 2015; Cámara, 2017); and 2) a narrower, northern retro-wedge in which the same cover is more internally deformed by north-vergent thrusts and long-wavelength folds (Gómez et al., 2002; Cámara, 2017). Beneath the salt décollement, the structure of the Basque Pyrenees consists of partially subducted Iberian

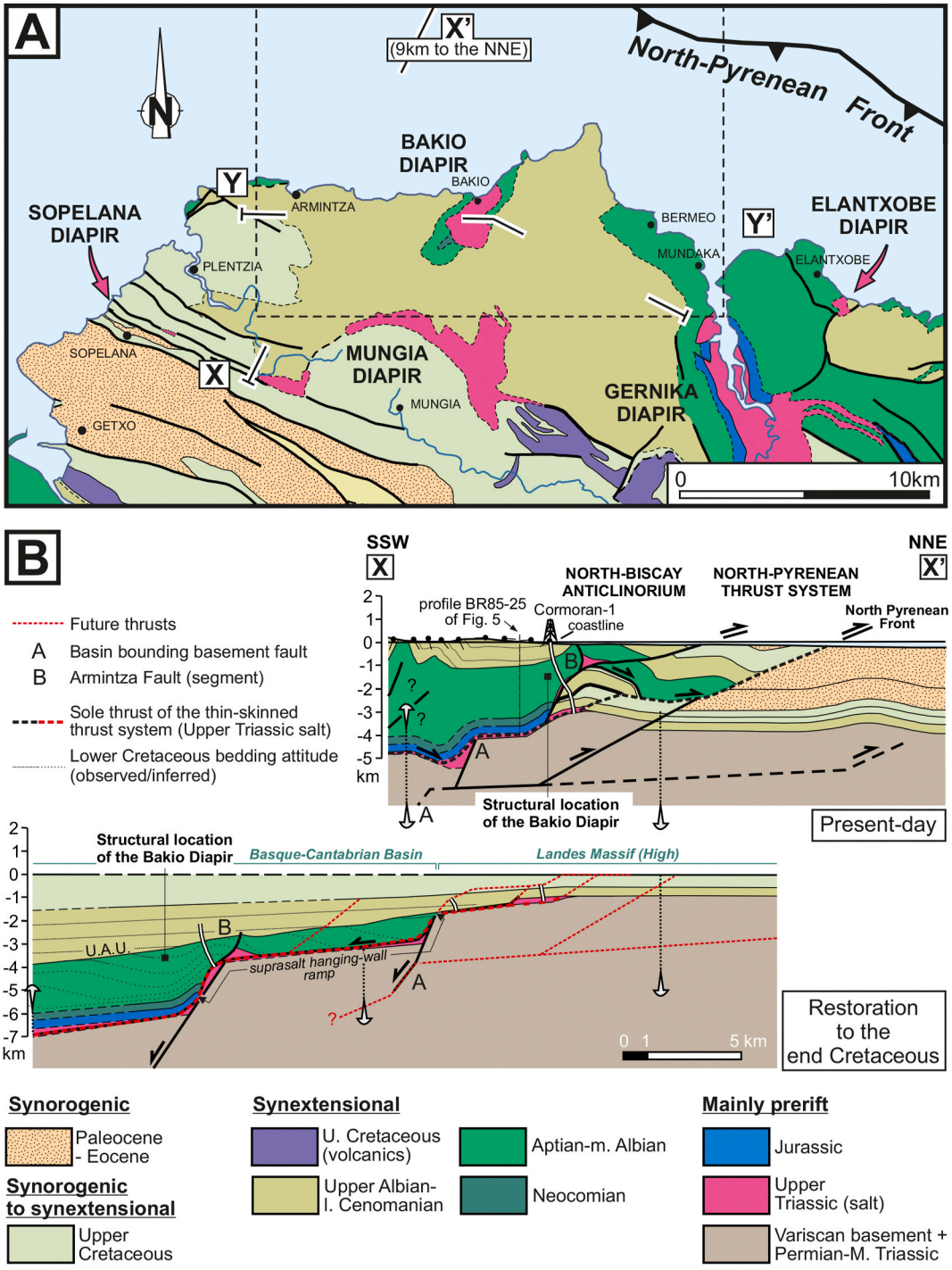

Fig. 3. A) Simplified geologic map of the onshore western terminations of the North-Biscay Anticlinorium and Biscay Synclinorium with the location of the Bakio Diapir. X-X': location of the cross section depicted in Fig. 3B (note that the northern end of this section is positioned 9 km NNE of the map). Y-Y': location of the seismic profile shown in Fig. 5. Dashed rectangle: location of the geologic map of Fig. 4. **B)** Balanced section across the North-Biscay Anticlinorium and North-Pyrenean Thrust System with a restoration to the end Cretaceous (North-Pyrenean foreland basin structure after Gómez et al., 2002). U.A.U.: Upper Albian Unconformity.

lithosphere beneath the Eurasia plate (Pedreira et al., 2003, 2007) in which the overriding plate was partially incorporated into the retro-wedge (Fig. 2B).

This decoupled architecture of the Basque Pyrenees was largely determined by the extensional structure of the precursor Basque-Cantabrian Basin. This consisted mainly of a major low-angle, north-directed extensional fault exhuming Iberian mantle in its footwall and a series of south-directed high-angle extensional faults affecting the upper crust of the Eurasian plate (Roca et al., 2011; Cámara, 2017). The basement extensional fault architecture was consequently distinct in the two basin margins, which in turn had a strong impact on the distribution and geometry of the stretched prerift Upper Triassic salt and, therefore, on the subsequent contractional deformation. In the northern basin margin, where the salt layer was vertically disrupted and drape folded by high-angle basement-involved faults, the cover deformation was distributed across a broad region with thin-skinned folds and thrusts usually nucleated over the subsalt extensional faults (Soler et al., 1981; Gómez et al., 2002; Quintana et al., 2015; Cámara, 2017; DeFelipe et al., 2018). In contrast, along the southern margin, where the stretched salt was distributed over a gentle low-angle detachment, the cover deformation concentrated at the frontal, southern tip of the salt detachment (Carola et al., 2015; Cámara, 2017).

Apart from the inherited extensional subsalt structure, the location and geometry of the Pyrenean cover deformation was also controlled by preexisting salt diapirs (Fig. 2). In most cases, these were passive diapirs during the Early Cretaceous to Santonian formation of the Basque-Cantabrian Basin (Brinkmann et al., 1967; Boess, 1984; Serrano and Martínez del Olmo, 2004; Klimowitz et al., 1999; Bodego and Agirrezabala, 2013; Poprawski et al., 2014; Frankovic et al., 2016). These precursor diapirs were squeezed and commonly welded during the Pyrenean shortening (Mathieu, 1986; García-Mondejar, 1987; Gómez et al., 2002; Cámara, 2017; Soto et al., 2017). In short, the crustal structure of the early rift history controlled the initiation and growth of salt diapirs, and both the extensional faults and associated diapirs strongly influenced the subsequent development of the Basque Pyrenees.

2.2. Extensional evolution

The extensional development of the Basque-Cantabrian Basin included two main evolutionary stages: latest Jurassic-middle Albian and late Albian to middle Cenomanian (Rat, 1988; Pedrera et al., 2017; García-Senz et al., 2019; Muñoz, 2019). The latest Jurassic-middle Albian stage was characterized by widespread stretching leading to the development of the Basque-Cantabrian Basin with the formation of basement-involved faults along its margins (Rat, 1959, 1988; García-Mondéjar and García-Pascual, 1982; Agirrezabala, 1996; Martín-Chivelet et al., 2002). The motion of these subsalt faults would have induced the development of monoclinal drape folds either above them or at relay ramps, with the salt accommodating the difference in geometry (Roca et al., 2011; Rowan, 2014; Carola et al., 2015, Fig. 3B, bottom). Because the suprasalt succession also had to be stretched, this drape folding was accompanied by suprasalt extensional faulting usually concentrated at the upper hinge of the monoclinal folds and relay ramps (Tavani and Granado, 2014; Carola et al., 2015). With enough extension relative to sediment accumulation, these were where most Basque-Cantabrian diapirs initiated by reactive diapirism (Bodego and Agirrezabala, 2013; Carola et al., 2015). During this time, the basin was gradually infilled by fluvio-deltaic and shallow marine siliciclastic sediments that graded basinwards to carbonate platforms and marly successions (Rat, 1959; Agirrezabala and García-Mondejar, 1989; García-Mondejar, 1989).

The late Albian to middle Cenomanian stage marked a significant change in the basin kinematics and dynamics. At this time, most upper crustal faults at the basin margins became inactive and lithospheric extension shifted toward the basin center and became focused on 1–2 major low-angle extensional lithospheric faults (DeFelipe et al., 2017; Muñoz, 2019). These faults, in some areas, accommodated the basinward displacement of the Mesozoic cover over the Upper Triassic salt resulting in: 1) thin-skinned salt-detached extensional deformation; and 2) the development of drape folds above the pre-existing basement faults, such as those described by Bodego et al. (2013, 2018) in the eastern Basque-Cantabrian Basin. Furthermore, during the beginning of this stage, the entire Basque-Cantabrian Basin was uplifted (García-Mondéjar et al., 1996, 2005; Bodego and Agirrezabala, 2013), giving rise to the erosion of the basin margins and, ultimately, of the salt inflated areas within the basin. The erosion of the basin margins (e.g., the north-fringing Landes Massif; Voort, 1964; Robles et al., 1989; Martín-Chivelet et al., 2002) resulted in a significant increase of terrigenous input into the Basque-Cantabrian Basin, which resulted in a change from predominantly carbonate to siliciclastic deposition (Wiedmann et al., 1983; García-Mondéjar et al., 1996, 2005; Bodego et al., 2015, 2018). This stage was coeval to lower crust (?)-mantle exhumation (Jammes et al., 2009; Tugend et al., 2014; DeFelipe et al., 2017). After this initial uplift, there was a significant increase of the subsidence of the entire Basque-Cantabrian Basin, which generated accommodation space that was only partially filled by terrigenous sediments coming from the basin margins (Martín-Chivelet et al., 2002; García-Modéjar et al., 2005; Bodego et al., 2015). Depositional environments graded rapidly basinwards from fluvial (Utrillas Fm.) to shelf with some deltas and, at the basin center, deepwater turbidite fans.

3. Data and methodology

This study is based on both surface and subsurface data. The onshore dataset comprises: a) 3533 bedding, fault, cleavage, and joint measurements collected using a compass along the Lemoniz-Mundaka coastline and the inland areas included in the map of Fig. 4; b) 161 bedding attitudes obtained from Airbone Lidar images of the studied coastline available at the webpage of geoEuskadi (ftp://ftp.geo.euskadi.eus/lidar); c) the bedding and geological information included in the EVE 1:25.000 scale geological maps of Armintza (37-II), Bermeo (38-1), Mungia (38-III) and Getxo (37-IV); and d) 11 sedimentary logs (4 measured in the field and 7 synthetic constructed from the lithological and bedding attitude observations done in isolated outcrops). All these data, together with field geological mapping of the coastline areas, have been used to produce the new geological maps presented in Fig. 4 and A of the supplementary data and to construct the cross sections included in the paper (Figs. 3 and 5).

Offshore, the surface geology has been inferred from the 1 m isobath-interval bathymetric map obtained by AZTI Tecnalia for the Eusko Jaurlaritza (available at http://www.geo.euskadi.eus/geograficos/batimetrias-marinas-pais-vasco-ano-2009/s69-geodir/es/webpage). This map, created using a multibeam echosounder and LIDAR bathymetric flights, shows five well-differentiated seabed morphological facies (A to E in Fig. 6). The bathymetric signature of each facies has been compared to the relief generated by the rocks exposed onshore along the non-vegetated coastline, and from this comparison, they have been correlated with reasonable confidence either with the Quaternary or with the four main onshore lithologic units (upper Albian-Cenomanian turbidites or Aptian-lower Albian marlstones, breccias, and platform carbonates).

The subsurface data include the Cormorán-1 exploratory well (see location in Fig. 4) and the time-migrated BR85-25 and BR85-26 reflection profiles. The Cormorán-1 well reached a depth of 2980 m and was drilled by RIPSA (REPSOL) in 1997. Its final report and dipmeter logs have been used to constrain the deep structure in the cross section of Fig. 3. The BR85-25 and BR85-26 seismic profiles were acquired in 1986 by CGS for ENIEPSA and are characterized by overall poor quality. They are combined here to produce a composite strike line (Fig. 5) that, going from the Jata-Gorliz Minibasin to the western flank of the Gernika Diapir, images some geometries of the deep structure of the flanking minibasins. These geometries include stratigraphic and tectonic contacts

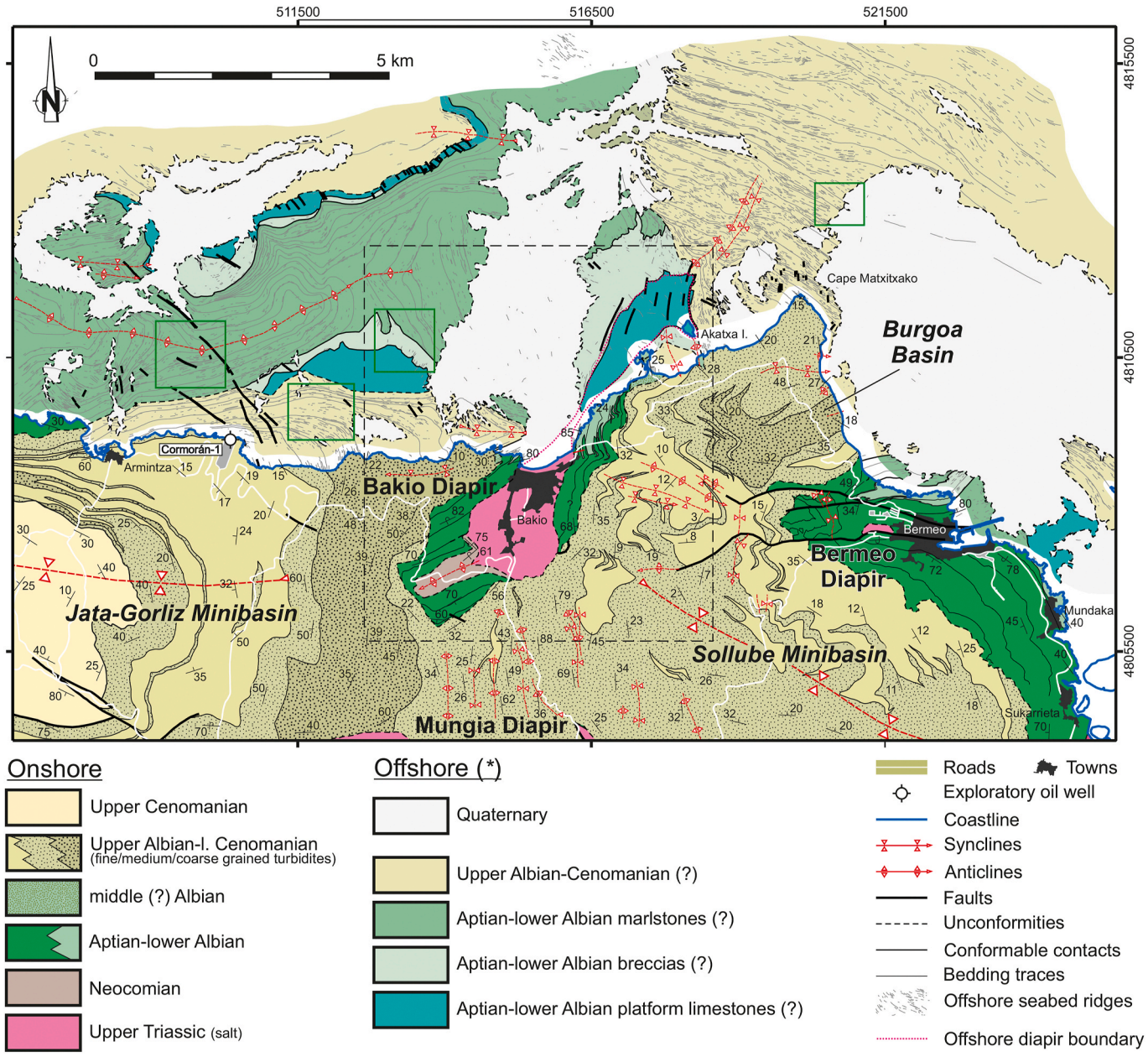

Fig. 4. Detailed geologic map of the study area. Westernmost and southeastern map areas based on EVE 1:25.000 scale geological maps of Armintza (37-II), Mungia (38-III) and Getxo (37-IV). Thick dark blue line with fringing white strip: present-day coastline and near-shore areas. Dashed rectangle: location of the geologic maps of Fig. 10. Offshore geology is from interpretation of the 1 m isobath-interval bathymetric map obtained by AZTI Tecnalia for the Eusko Jaurlaritza. Green rectangles: location of the seabed bathymetric images shown in Fig. 6. *: Age attribution and geological mapping of the offshore units based on the morphological features and distribution of the 5 rocky seabed bathymetric facies described in Fig. 6. (For interpretation of the references to color in this figure legend, the reader is referred to the Web version of this article.)

that have been depth converted using average interval velocities obtained from velocity surveys of the wells Cormorán-1, Alda-1, Antezana-1, San Antonio-1, Marinda-1, Gastaín-1, Zúñiga-1, and Castillo-2 (see Fig. B of supplementary data). Along the profile, the surface geology defines the contacts of the Aptian to lower Albian successions. Below, the Upper Triassic, Jurassic, and Neocomian tops have been tied to outcrops on the western flank of the Gernika Diapir and extended westwards following reflectors and applying seismic facies criteria. This last criterium appears particularly reliable for defining the top and bottom of the Lower-Middle Jurassic, which throughout the entire Pyrenean realm is imaged as a characteristic high-amplitude reflectivity package stratigraphically bounded upwards and downwards by transparent reflective facies belonging respectively to the Upper Jurassic marly successions and Upper Triassic salt (Serrano and Martínez del Olmo, 1990; Carola et al., 2015; Muñoz et al., 2018).

The cross-section restoration in Fig. 3 was constructed using the Move software and restored using the bed-length method, which models deformation by flexural slip. Bed thicknesses have been maintained in the sequential restorations because no decompaction corrections have been applied. Consequently, the presented restorations must be considered semi-quantitative.

4. The structure of the Basque-Cantabrian Basin in the Bakio area

The Bakio Diapir formed close to the northern edge of the Basque-

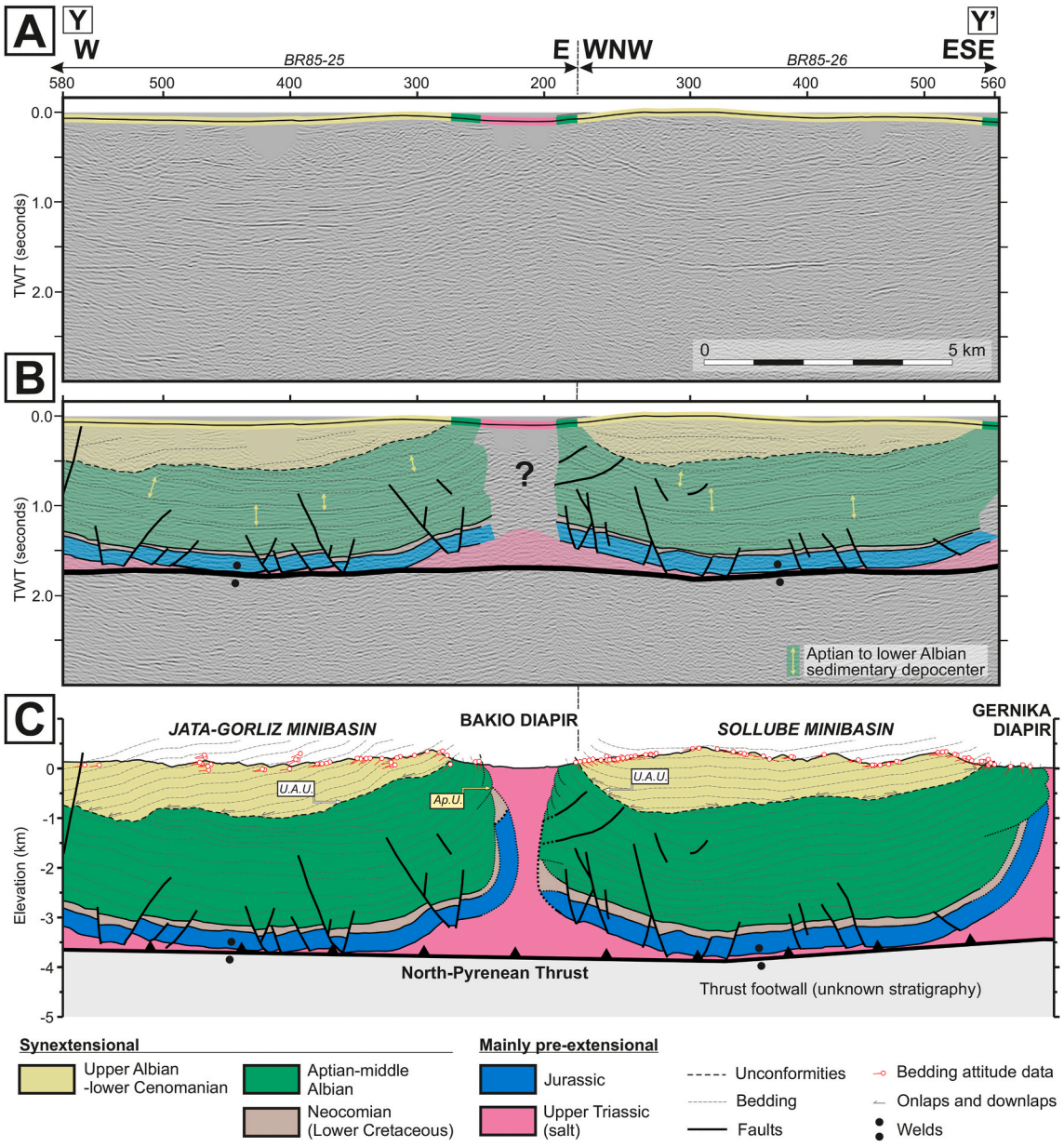

Fig. 5. E-W to WNW-ESE (strike) transect across the Bakio Diapir. **A)** Uninterpreted time-migrated composite seismic section formed by the BR85-25 and BR85-26 profiles; colors at top indicate exposed geologic units. **B)** Interpretation of the composite seismic section. **C)** Depth-converted geologic cross section based on the interpreted seismic section (B) and the surface geology (no vertical exaggeration). Wider dashed lines close to the diapirs: structure of the diapir-flanking rocks inferred from surface geological maps (i.e., location of the Ap.U. at the western edge of the Bakio Diapir which, according to the geological map of Fig. 4, is stratigraphically located about 600–700 m beneath the surface trace of the U.A.U.). Depth conversion generated using average interval velocities obtained from velocity surveys of the wells Cormorán-1, Alda-1, Antezana-1, Sant Antonio-1, Marinda-1, Gastaín-1, Zúñiga-1, and Castillo-2 (see Fig. B of supplementary data). U.A.U.: Upper Albian Unconformity; Ap.U.: Intra-Aptian Unconformity. Location of seismic profile shown in Fig. 3 (Y-Y′). (For interpretation of the references to color in this figure legend, the reader is referred to the Web version of this article.)

Cantabrian Basin (Fig. 2). As with other diapirs located along this basin margin, it is a salt wall that was passively transported towards the north in the hanging wall of the northern frontal thrust system during the Pyrenean orogeny (Feuillée and Rat, 1971; Ferrer et al., 2008; Quintana et al., 2015; Ábalos, 2016). This thrust system emerges along the modern offshore Basque shelf close to the coast, 6–8 km north of the Bakio Diapir (Soler et al., 1981; Sanchez, 1991; McDougall et al., 2009, Fig. 3).

The structure and age of the footwall of this thrust system is unknown beneath the Bakio Diapir. Further north, the available seismic data show that its structure is rather simple and consists of a nearly horizontal plateau affected by some minor north-directed thrusts and folds (Fig. 3; Ferrer et al., 2008). Exploration wells in this plateau show that the upper Albian-middle Cenomanian sandstones and the upper Cenomanian limestones unconformably overlie the Paleozoic basement of the Landes Massif (Gariel et al., 1997; Gómez et al., 2002; Ferrer et al., 2008; McDougall et al., 2009; Pedrera et al., 2017). The Triassic to middle Albian succession is missing. This Mesozoic stratigraphy contrasts with that of the overlying North-Pyrenean thin-skinned thrusts, which includes a thick Triassic to middle Albian succession, thereby demonstrating that the northern Pyrenean thrust system reactivated the northern rift margin of the Basque-Cantabrian Basin (Fig. 2).

In the study area, the north Pyrenean frontal thrust system is detached in the Upper Triassic salt as shown by the well data (Fig. 3) and has a minimum displacement of about 10–15 km (Gómez et al., 2002).

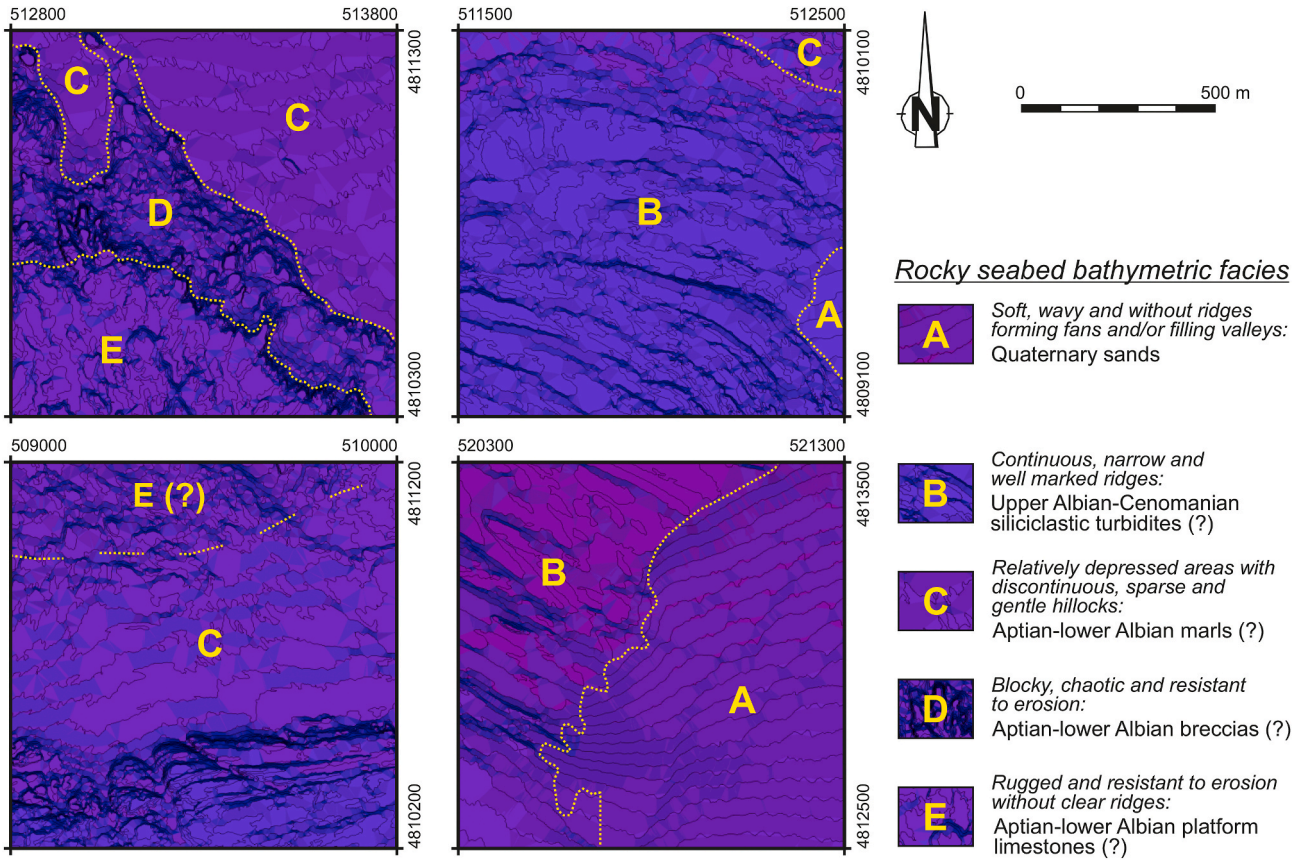

Fig. 6. Rocky seabed bathymetric facies distinguished in the 1 m isobath-interval bathymetric map obtained by AZTI Tecnalia for the Eusko Jaurlaritza using a multibeam echosounder and LIDAR bathymetric flights (available at http://www.geo.euskadi.eus/geograficos/batimetrias-marinas-pais-vasco-ano-2009/s69-geo-dir/es/). Age atribuction of each differentiated bathymetric facies based on the relief of each onshore unit along the present-day intertidal zone.

The Cormorán-1 well drilled three repeats of the upper Albian-middle Cenomanian stratigraphy (Fig. 3). In the upper two imbricates, the Aptian-middle Albian synrift sediments are directly on top of the Triassic evaporites, whereas in the footwall these synrift sediments are missing. Again, these relationships demonstrate the contractional reactivation of Early Cretaceous extensional faults at the northern margin of the Basque-Cantabrian Basin. The restored cross section (Fig. 3B, bottom) shows a major décollement at the Upper Triassic salt that decoupled the extensional deformation. The suprasalt section is only drape folded above the major basement extensional faults, with significant suprasalt extension located north of the BR85-25 seismic profile close to northern basin margin (Fig. 3B). In this area, the Jurassic-Lower Cretaceous succession shows a broad hanging wall ramp. Its length of about 10 km is a maximum estimate of the suprasalt stretching (Fig. 3B).

Abrupt changes in the stratigraphic thicknesses of the hanging-wall strata of the thin-skinned thrust sheets (Fig. 3) record the presence of two major subsalt ENE-trending basement extensional faults that, in the study area, marked the northern margin of the Basque-Cantabrian synrift basin. The outermost fault, bounding the Aptian-lower Albian syn-extensional deposits, has a throw of about 1.5 km (fault A in Fig. 3); and the second (fault B in Fig. 3), located some 9–10 km basinwards (south), has 2–2.5 km of throw.

The stretched Jurassic-Cretaceous basin infill is pierced by salt walls similar to Bakio, but with diverse orientations (Sopelana, Munguia, Gernika, Bermeo, etc.), that are linked by narrow corridors where the suprasalt cover is strongly deformed by contractional structures (Figs. 4 and 7A). These corridors are characterized by short-wavelength folds, suggesting that they formed over preexisting salt ridges in which the suprasalt cover was thinner. These salt ridges, together with the diapirs, form a polygonal pattern that separates elliptical to polygonal minibasins (Fig. 7) in which the Cretaceous infill is only slightly deformed, with bowl-shaped stratal geometries and wide, moderately dipping limbs (<35°; Fig. 5). The origin of the diapirs and linking ridges is not well constrained with the available data since the older syn-diapiric deposits are rarely exposed. However, they mostly parallel the extensional basement faults that bound the Basque-Cantabrian Basin as well as thin-skinned faults cropping out west of Armintza (Robles et al., 1988), and passive diapirism was ongoing prior to shortening. Thus, we infer that most diapirs and linking salt ridges were established by motion on the extensional faults.

The Bakio Diapir is located between the Burgoa rollover extensional basin and the Sollube and Jata-Gorliz minibasins (Figs. 4, 5 and 7) at the junction of three salt ridges. One, located offshore just NW of the exposed diapir, is not very obvious. It corresponds to the ENE prolongation of the Lower Cretaceous extensional fault system recognized west of Armintza by Robles et al. (1988) and is indicated by a wide isolated area of massive and resistant rocks at the sea floor that we interpret as carbonate platform rocks (Fig. 4). The other two ridges are located onshore and recorded by two prominent corridors in which: 1) the Lower Cretaceous is strongly deformed by tight short-wavelength folds and some minor thrusts; and 2) there could be welded salt diapirs (Bermeo Diapir) (Figs. 4 and 7). One of these ridges is roughly parallel to the basin margin and links the Bakio and Gernika diapirs; the other trends N-S and connects the Bakio and Mungia diapirs (Fig. 7).

The two salt ridges parallel to the basin margin separate Lower Cretaceous successions that are much thicker in the south than in the north. Thus, as shown in Fig. 3B, they record underlying basement-involved faults dipping towards the SSE (Bermeo and Armintza faults in Fig. 7B). The pattern suggests that the Bakio Diapir formed at a relay ramp connecting these two right-stepping en-echelon faults (Fig. 7).

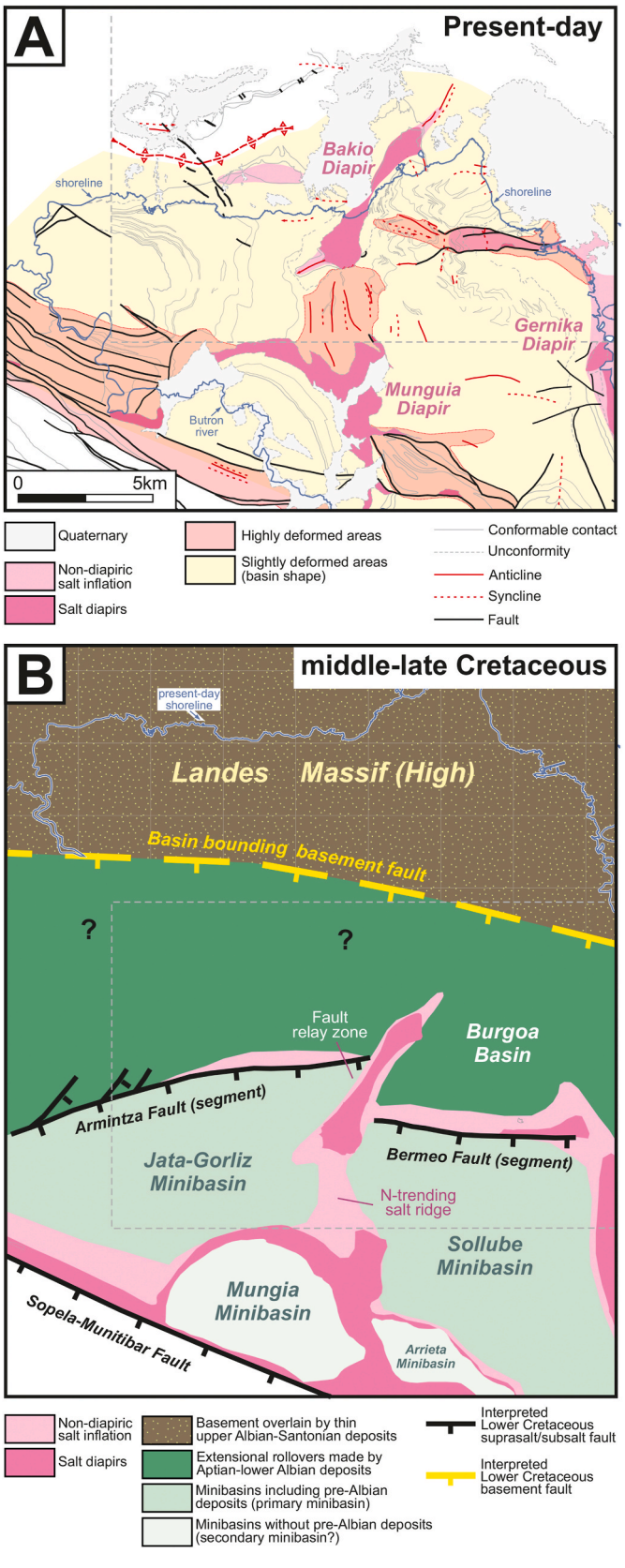

(caption on next column)

Fig. 7. A) Present-day structure map of the western end of the North-Biscay Anticlinorium with the distribution of inflated salt areas and areas of overburden that are highly or slightly deformed. Highly deformed: Cretaceous and Paleogene rocks affected by pervasive thrusts and tight folds (bedding attitudes >50°). Slightly deformed: Jurassic to Paleogene rocks forming basin geometries with predominant bedding attitudes <40°. The map has been generated by superposing the geologic map of Fig. 4 (rectangular area bounded by the dashed thin grey line) upon a regional one built from the geologic 1:25.000 EVE and 1:50.000 IGME maps. **B)** Structure map prior to Pyrenean shortening highlighting the inflated salt areas, minibasins, and faults active during the Early Cretaceous. These faults have been inferred from both the distribution of different magnitudes of deformation and sharp Lower Cretaceous thickness/lateral facies changes. Note that: 1) the width of the salt diapirs clearly is underestimated and had to be greater since diapir squeezing during the Pyrenean orogeny has not been removed; and 2) the suprasalt structures have moved 13 km southwards in order to restore the estimated north-directed Pyrenean thrust displacement. Dashed thin grey line: restored location of the boundaries of the salt and suprasalt successions mapped in Fig. 4.

Accordingly, the N-trending salt ridge extending south from the relay ramp and Bakio Diapir is interpreted as a displacement-gradient anticline formed adjacent to the paleo-fault tips (see Kane et al., 2010, and Wilson et al., 2013, for descriptions of such anticlines).

This interpretation of the N-trending ridge is compatible with the geometry observed on the seismic profile (Fig. 5) oriented along the strike of the hanging wall of both S-dipping basement faults. The Bakio Diapir is flanked on both sides by two minibasins of similar thickness above welds with the same structural elevation. Thus, the diapir/ridge was not linked to the presence of a N-trending basement-involved fault. Also, it is consistent with the position of the Bakio Diapir at the northern end of this ridge, where two factors may have contributed to diapir initiation. First, basement folds induced by the displacement gradients on the two faults would have had a larger amplitude (Kane et al., 2010; Wilson et al., 2013), which in turn implies a locally thinner roof above the salt. Second, there may have been excess extensional strain due to drape folding not just to the S over the basement faults, but also to the WSW from the footwall of the Bermeo Fault to the hanging wall of the Armintza Fault (Fig. 7B). Associated extensional faults formed by stretching of suprasalt strata (Fig. 5) might have triggered reactive diapirism.

5. The Bakio Diapir

5.1. The diapir and overburden stratigraphy

The Bakio Diapir is recorded at the surface by isolated outcrops of massive sub-volcanic tholeiitic rocks termed ophites (Béziat et al., 1991) and by highly deformed red claystones cut by plentiful secondary gypsum veins (Fig. 8). Upper Triassic in age, these rocks represent the insoluble residue of a layered evaporite sequence that, penetrated by several wells in the region, comprises mainly halite with minor proportions of anhydrite, red claystones, and ophites (Hempel, 1967; Lanaja, 1987; Serrano and Martínez del Olmo, 1990; Frankovic et al., 2016; Cámara, 2020). Thus, the exposures represent caprock formed by weathering and halite dissolution.

Above and flanking the diapir, the overburden is divided into four major stratigraphic units (Fig. 9).

5.1.1. Jurassic

The lowest unit, pre-diapiric and Jurassic in age, does not crop out in the study area but is well exposed on the flanks of the neighboring Gernika Diapir (Fig. 3). There, it consists of a ~300–400 m thick succession of basal dolostones, marlstones, and oolitic limestones deposited in a marine carbonate ramp environment (Soler and José, 1972; Boess, 1984).

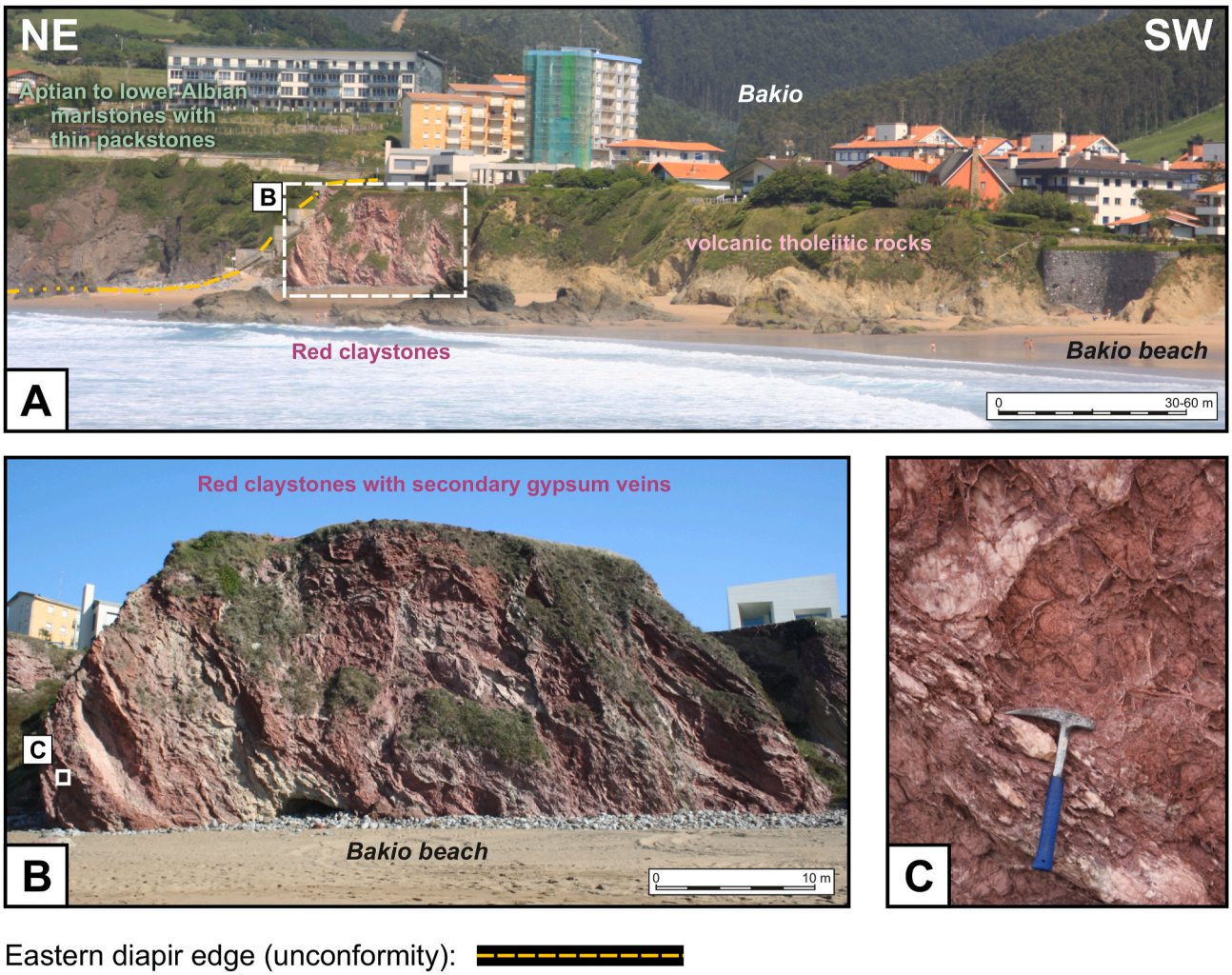

Fig. 8. A) Photograph looking E of the Bakio Diapir and flanking Aptian to lower Albian marly successions at the Bakio beach. The diapir is recorded by sub-volcanic tholeiitic rocks (green to ocre outcrops on the beach) and rey claystones cut by plenful secondary gypsum veins (red outcrops). The Aptian to lower Albian succesions at the NE edge of the photograph dip towards the diapir with overturned polarity. Dashed white line in the photograph: area covered by Fig. 8B. **B)** Detail of the Upper Triassic red claystones with pervasive system of gypsum veins which predominantly dip southwestwards. **C)** Closer view of the same diapir rocks. See white circle in Fig. 8B for location. (For interpretation of the references to color in this figure legend, the reader is referred to the Web version of this article.)

5.1.2. Neocomian

Unconformably overlying the Jurassic carbonates, the second unit has also been described in the same diapir flanks. It is formed by a 90–120 m thick succession of Neocomian epicontinental black, shell-rich limestones and marlstones that become more sandy and rich in orbitolinids up-section (Soler and José, 1972; Espejo et al., 1975). Although not identified previously in the Bakio area, this unit is interpreted here to be present at the SW edge of the Bakio Diapir where similar black marly mudstones and sandstones rich in orbitolinids appear beneath the Aptian marly succession (Fig. 4). The Neocomian sediments are the oldest synrift rocks observed in the study area. However, due to the lack of clearly halokinetic features, we consider it as synrift, but pre-passive diapirism.

5.1.3. Aptian-middle Albian

The overlying other two Cretaceous units, in contrast, are clearly syn-passive diapirism (Rowan et al., 2012b; Ferrer et al., 2014; Poprawski et al., 2014, 2016; Cumberpatch et al., 2020). The older one, Aptian to middle Albian in age, is up to 2500 m thick (Fig. 5) and fringes most of the exposed salt diapir. It comprises the Urgonian Group and the Punta Bakio unit of the Black Flysch Group (Fig. 9) defined by Poprawski et al. (2014; 2016). This unit is composed of marine carbonates and subordinated siliciclastic turbidites deposited in a platform to slope environment displaying deepening upward facies (García-Mondejar and Robador, 1987; Robles et al., 1988). On the flanks of the Bakio Diapir it can be divided into lower and upper carbonate successions (Figs. 9 and 10A) whose boundary, not well defined with biostratigraphic data, is located in the latest Aption or earliest Albian times.

The lower carbonate succession crops out along the central and southern part of the western diapir edge and, on the eastern side, in a small outcrop at the end of the Bakio beach (Fig. 8). It is $>$ 700 m thick and consists of outer-shelf marlstones and marly limestones with periodic thin-bedded packstones.

The upper carbonate succession is approximately 500 m thick and is well represented along both diapir margins. Unlike the underlying unit, it is lithologically highly variable. It is formed by basinal marlstones that grade northwards to outer-slope marly limestones and marlstones with resedimented carbonate breccias and slumps and, closer to the diapir edges and roof, to platform rudistid limestones (García-Mondejar and Robador, 1987; Robles et al., 1988; Ferrer et al., 2014; Poprawski et al., 2014, 2016). This carbonate succession grades upwards into an 30–70 m thick sequence (Punta Bakio unit of Robles et al., 1988, and Poprawski et al., 2014) with an increasing amount of siliciclastic deposits that crop out along the coastline on both flanks of the diapir. The siliciclastic

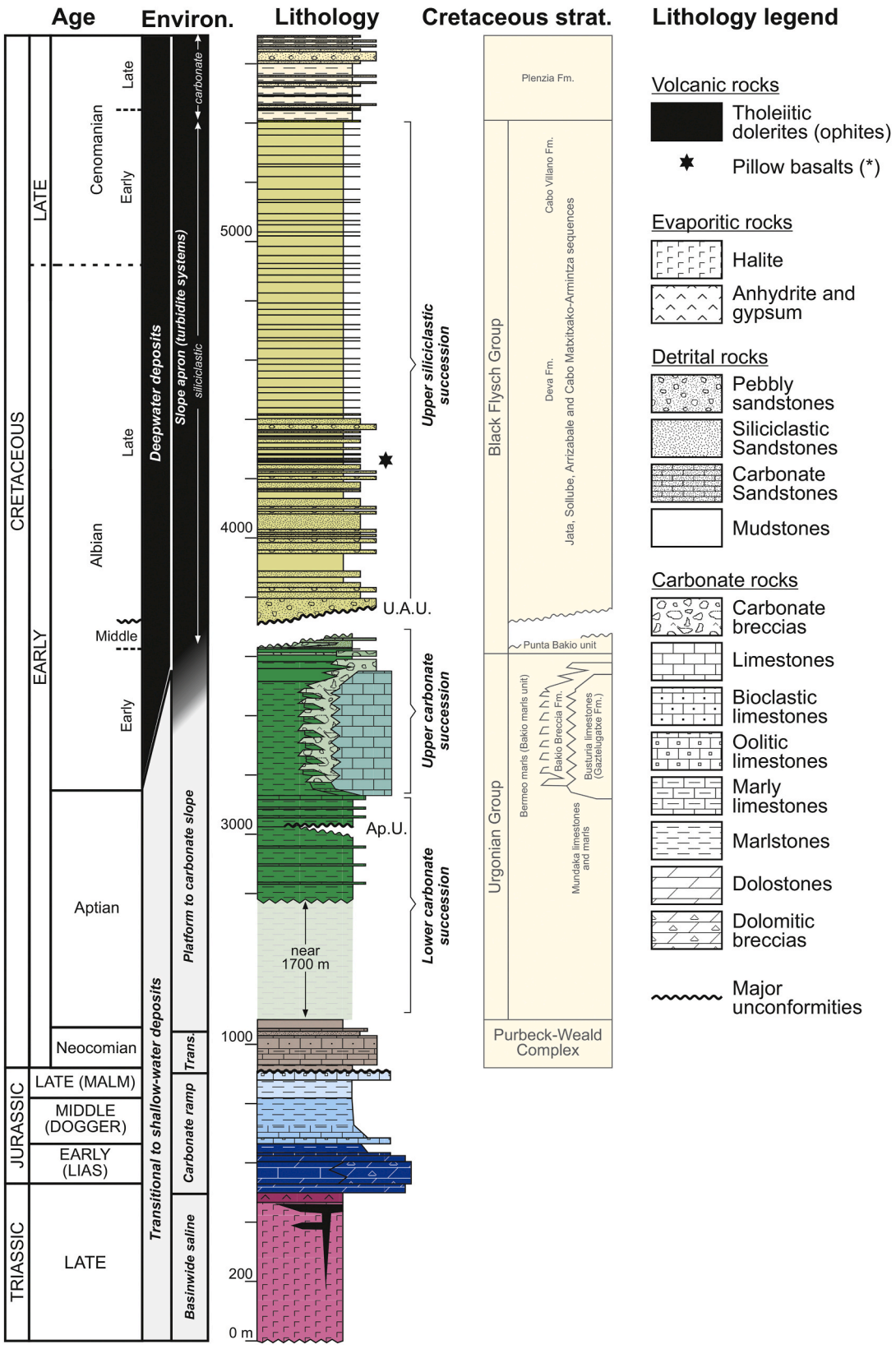

Fig. 9. General stratigraphic section of the study area with the main lithologies and depositional environments (based on Espejo et al., 1975; Boess, 1984; García-Mondejar and Robador, 1987; Robles et al., 1988; López-Horgue et al., 2009; Poprawski et al., 2014; and stratigraphic sections done in this study). Cretaceous thicknesses are merely an average since they can vary significantly within the study area. Cretaceous stratigraphic units previously used in the study area by Rat (1959), García-Mondejar and Robador (1987), Mathey (1987), Robador and García-Mondejar (1987), Robles et al. (1988), Poprawski et al. (2014; 2016) are shown in grey, with the ones defined by the latter authors indicated in brackets. *: pillow basalts present at Armintza harbor and Portume cape (Bakio), dated by López-Horgue et al. (2009). U.A.U.: Upper Albian Unconformity; Ap.U.: Intra-Aptian Unconformity.

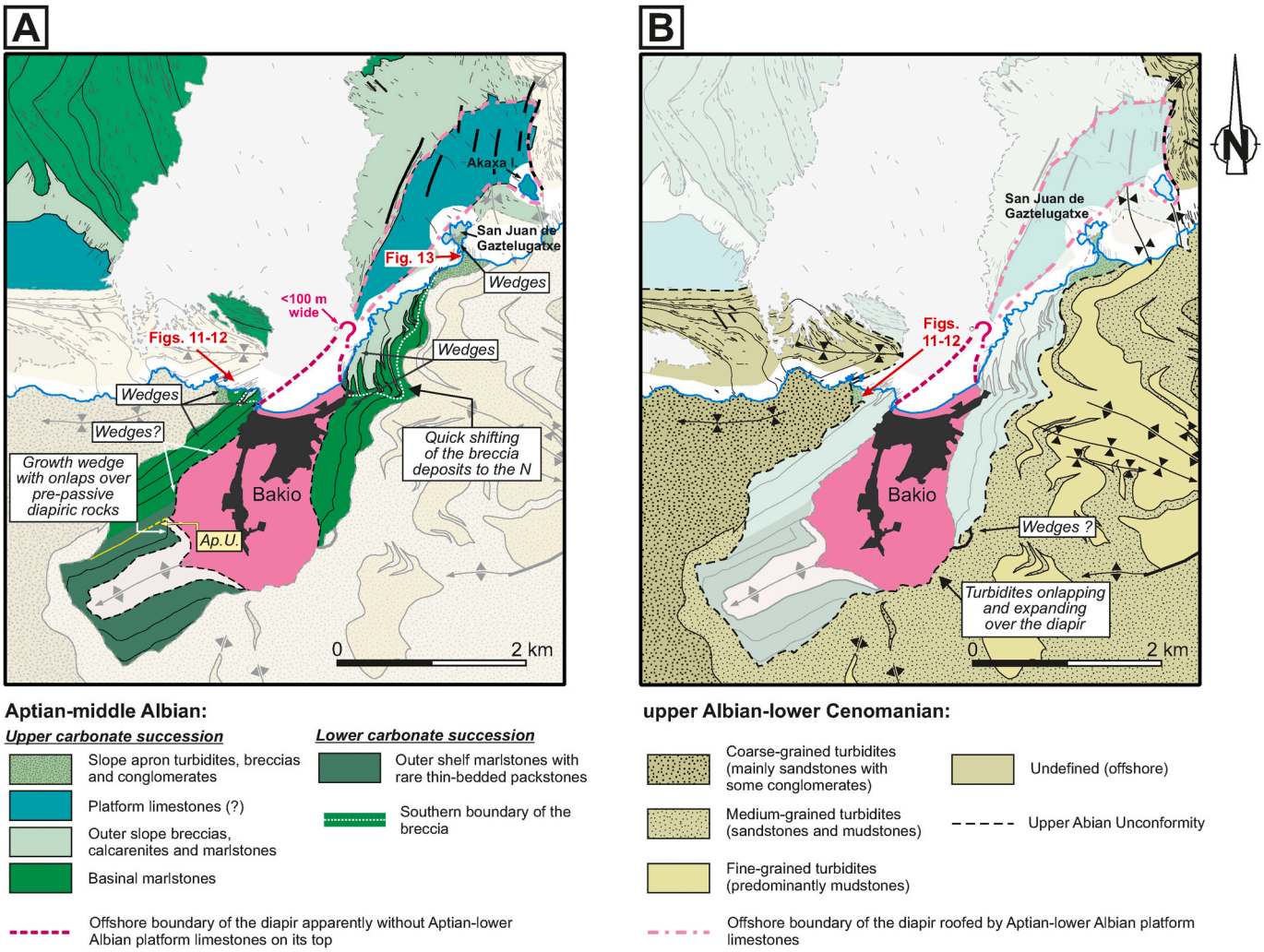

Fig. 10. A) Geologic map of the Bakio Diapir highlighting the Aptian-middle Albian successions and their main halokinetic features. Ap.U: intra-Aptian unconformity (base of the halokinetic sequences in direct contact with the salt). The location of the boundary between the Upper and Lower carbonate succesions at the western diapir side is approximative and based on the thickness of the breccias in the eastern side. **B)** Geologic map of the Bakio Diapir highlighting the upper Albian-lower Cenomanian successions and their main halokinetic features.

deposits consist of turbidites alternating with mudstones and abundant carbonate grainstone to mass-transport deposits mainly derived from a more or less lithified Aptian-middle Albian carbonate platform (Poprawski et al., 2016; Cumberpatch et al., 2020). These carbonate debrites consist, on the western diapir flank (Figs. 11 and 12), of: 1) thin and discontinuous lenticular bodies of carbonate clast- and matrix-supported breccias; 2) pebble calciturbidites; and 3) sandy grainstones directly above the breccias and calciturbidites. On the eastern flank, in contrast, the debrites comprise clast- and matrix-supported carbonate breccias and folded sandy grainstone beds incorporated into slumps (Fig. 13) which show a SE transport direction, i.e., perpendicular to the diapir edge (Poprawski et al., 2014, 2016).

5.1.4. *Upper Albian-lower Cenomanian*

The upper unit preserved in the study area (Fig. 4), late Albian-early Cenomanian in age, is essentialy siliciclastic and includes the Deva and Cabo Villano formations of the Black Flysch Group (Fig. 9). The thickness of this unit is difficult to determine because its top is only preserved to the west in the Jata-Gorliz Minibasin out of the study area (Fig. 4). Measured stratigraphic sections in the Sollube Minibasin indicate that it is thicker than 1050 m in the north (Robador and García-Mondejar, 1987; Arbués et al., 2012) and at least 1600 m thick in the south (Vicente-Bravo and Robles, 1991a). However, these values must be treated with caution since this unit shows an irregular base with significant onlap (Fig. 5).

The upper Albian-lower Cenomanian unit records a significant input of siliciclastic sediments into the Basque-Cantabrian Basin (García--Mondejar et al., 1996; Martín-Chivelet et al., 2002; García-Mondejar et al., 2005; Bodego et al., 2015) and is coeval with a global sea-level rise (De Graciansky et al., 1998; Haq, 2014). It consists of siliciclastic gravity-flow deposits with small proportions of mudstones, marlstones, and thin-bedded calciturbidites. Mass-transport deposits are also present but are restricted to minibasin margins and the lower part of the succession (i.e, in Armintza harbor, near San Juan de Gaztelugatxe, or along the east Matxitxako Cape coast), and contain redeposited Aptian to middle Albian platform sediments (Robador and García-Mondejar, 1987; Arbués et al., 2012; Poprawski et al., 2016).

The turbidite succession comprises black mudstones with siderite concretions, sandstones, and conglomerates. It has been divided into several sequences/units characterized by different predominant facies associations: amalgamated thick-bedded coarse-grained siliciclastic turbidites (Cabo Matxitxako-Armintza sequence/unit); thin-bedded and fine-grained siliciclastic turbidites interbedded with marlstones (Sollube sequence/unit); or both kinds of facies along with mass-transport deposits (Jata Sequence/unit) (Robador and García-Mondejar, 1987; Robles et al., 1988, 1989; Vicente-Bravo and Robles, 1991a; Poprawski

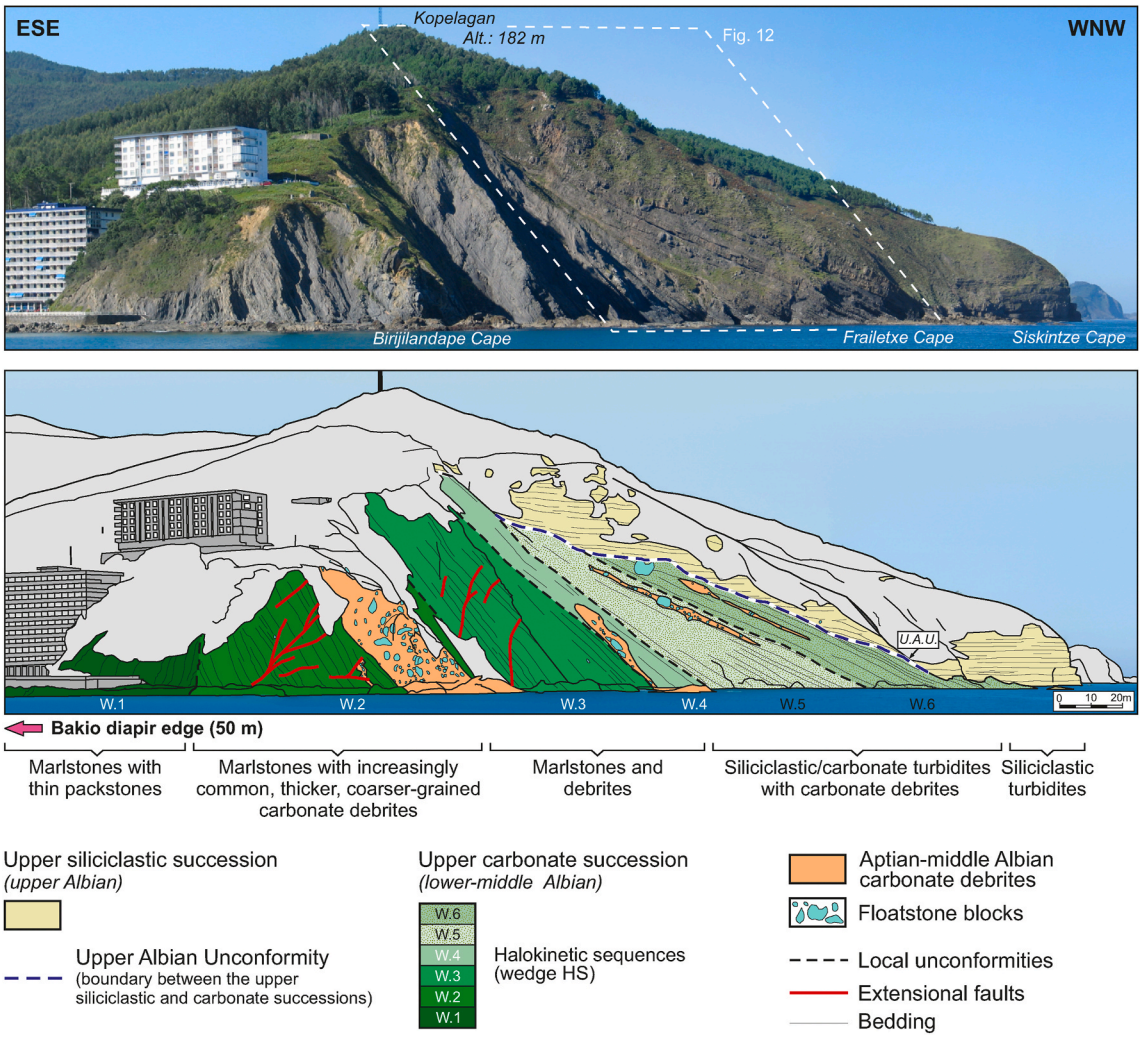

Fig. 11. Photograph looking SW and interpretation of the western flank of the Bakio Diapir at the coastline. Note the tapered geometry of the Aptian-middle Albian sequences and the major Upper Albian Unconformity that is onlapped by siliciclastic upper Albian turbidites. Thin dashed white line in the photograph: area covered by Fig. 12. W.1-W.6: Aptian to middle Albian unconformity-bound halokinetic sequences recognized at the coast in the western flank of the Bakio Diapir.

et al., 2016). Their areal extent, as well as measured paleocurrent directions and sedimentological features, denote that the upper Albian-lower Cenomanian turbidites were deposited in several north-to east-sourced deep-sea fans located at slope aprons (Amiot, 1982; Vicente-Bravo and Robles, 1991a, 1991b; Floquet, 2004).

The bottom of this unit is an angular unconformity that truncates Upper Triassic to middle Albian rocks (Figs. 4 and A of supplementary data). This major unconformity, herein named the Upper Albian Unconformity (U.A.U.; Fig. 9), is not exclusive to the Bakio area. It is a regional feature, also present at most margins and salt inflated areas of the Basque-Cantabrian Basin (García-Mondejar, 1982; Boess, 1984; Fernández-Mediola et al., 1993; García-Mondejar et al., 1996; Agirrezabala et al., 2002; Pujalte and Robles, 2008; Bodego and Agirrezabala, 2013; Barrón et al., 2015; Bodego et al., 2015). There is consensus in the literature that the unconformity is related to a sea level drop and a sudden change in the tectonic evolution of the Basque-Cantabrian Basin (e.g., Robador and García-Mondejar, 1987; Robles et al., 1988), but not on the nature of this tectonic change. For Rowan (2014), it was associated with the transition from crustal thinning to exhumation during lithospheric extension. Alternatively, other authors link it to a dramatic decrease of the extension rate (Roca et al., 2011), a transpressional basin inversion (Souquet and Peybernés, 1991; García-Mondejar et al., 2005), the onset of thin-skinned extension (Bodego and Agirrezabala, 2013), or even to halokinetic processes (García-Mondejar, 1982; Ferrer et al., 2014; Poprawski et al., 2014).

5.2. Diapir structure

The BR85-25 and BR85-26 seismic profiles display the base of the Bakio Diapir at depth as well as the geometries of the adjacent minibasins (Fig. 5). The diapir pedestal, and thus the depth to the bottom of the salt that coincides with the sole thrust, is indicated by a divergence of reflections at 3.5–4 km beneath the Bakio Diapir. In the adjacent minibasins, extensional faults dipping mostly towards the diapir affect the Jurassic to middle part of the Aptian-middle Albian package, and, at the eastern edge of the diapir, slightly younger strata. In the eastern (Sollube) minibasin, westward depocenter migration (Fig. 5B) indicate differential salt evacuation that shifted towards the diapir.

The surface and near-shore data show that the Bakio Diapir is a 6.5–7.3 km long and <1.5 km wide NNE-trending salt wall with two outward plunging anticlines at its ends (Fig. 4). The geometry suggests that the salt wall was squeezed during the contractional Pyrenean deformation, albeit at an oblique angle due to its orientation relative to the shortening direction. This is compatible with its "Q-tip" map-view geometry, which is typical of squeezed salt walls (Rowan and Vendeville, 2006). Indeed, the salt wall is very narrow (<100 m) in the center, northeast of the Bakio beach, and becomes progressively much broader towards the two terminations where, at the surface, the diapir is 1–1.5

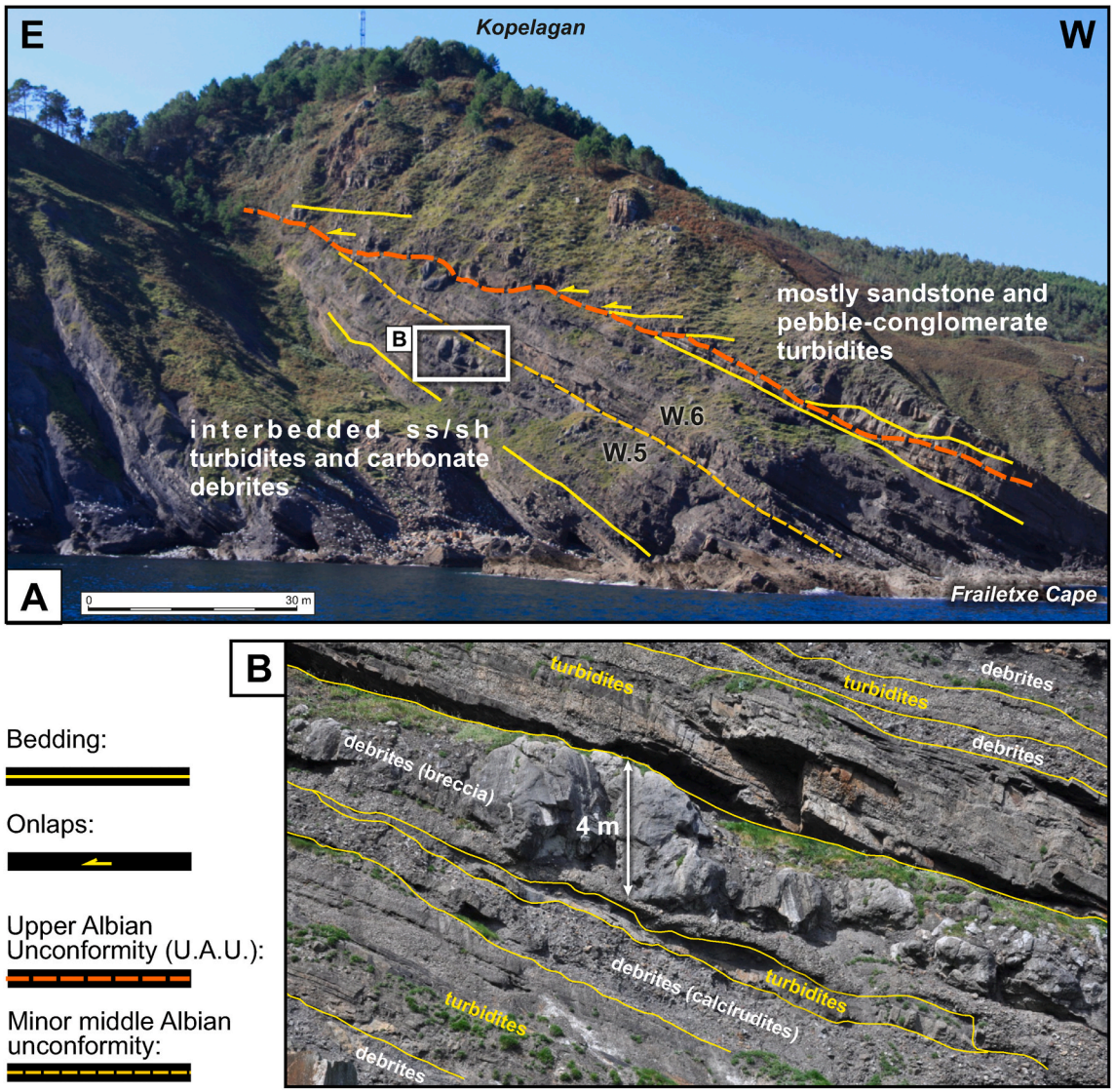

Fig. 12. A) Photograph looking south showing middle-upper Albian successions and unconformities on the western flank of the Bakio Diapir. W.5 and W.6: middle Albian halokinetic sequences recognized at the coast in the western flank of the Bakio Diapir. See Fig. 11 for location. **B)** Detail of the successions underlying the Upper Albian Unconformity that comprise an alternation of siliciclastic turbidites and carbonate debrites deriving from the Aptian-lower Albian platform capping the diapir. The debrites are composed mostly of calcirudites and clast-supported breccias with heterometric floatstone blocks up to 4 m in diameter.

km wide (Fig. 4).

This inferred squeezing is shown on the seismic cross section (Fig. 5), with the salt wall formed by a triangular pedestal and a bulbous crest separated by a narrow stem. This stem could be up to 400 m wide near the salt wall terminations, as in this section, but not in the center where there is no room to place a salt stem wider than 100 m (Fig. 4). Here, the diapir may be so narrow that it might even be welded. In any case, the narrow width of the diapir stem at the center of the salt wall is consistent with the results of an Anisotropy of Magnetic Susceptibility study carried out in the onshore diapir flanks (Soto et al., 2017). This analysis showed that the contractional deformation was transmitted from the SE diapir edge to the NW one in the center of the salt wall but not in the adjacent wider diapir areas. Here, unlike the center of the salt wall, the magnetic lineations (main stretching direction) are not perpendicular to the regional shortening direction on both diapir sides. Instead, the NW flank preserves an undefined or diapir-perpendicular magnetic orientation acquired during the pre-orogenic passive growth of the diapir (Soto et al., 2017).

6. The halokinetic architecture of the syn-diapiric deposits at the Bakio Diapir

The Aptian to upper Albian successions flanking the Bakio Diapir display a halokinetic-influenced architecture that varies upward. In this sense, we can distinguish three unconformity-bound packages that record different stages of the diapir growth: the lower Aptian, the upper Aptian-middle Albian and the upper Albian packages. The halokinetic architecture of these three packages as well as the features of the bounding unconformities are described below.

6.1. *Halokinetic architecture of the lower Aptian package*

The lower Aptian package includes the lower part of the lower carbonate succession, with the geometry observed at the southwestern diapir termination (Figs. 5 and A of the supplementary data). Here, it consists of a growth wedge of marly strata that onlaps an overturned panel of pre-passive diapiric Neocomian rocks (Figs. 4 and 10A, and A of the supplementary data). Thus, it is a package that recorded rotation of the Jurassic-Neocomian overburden, probably due to drape folding of

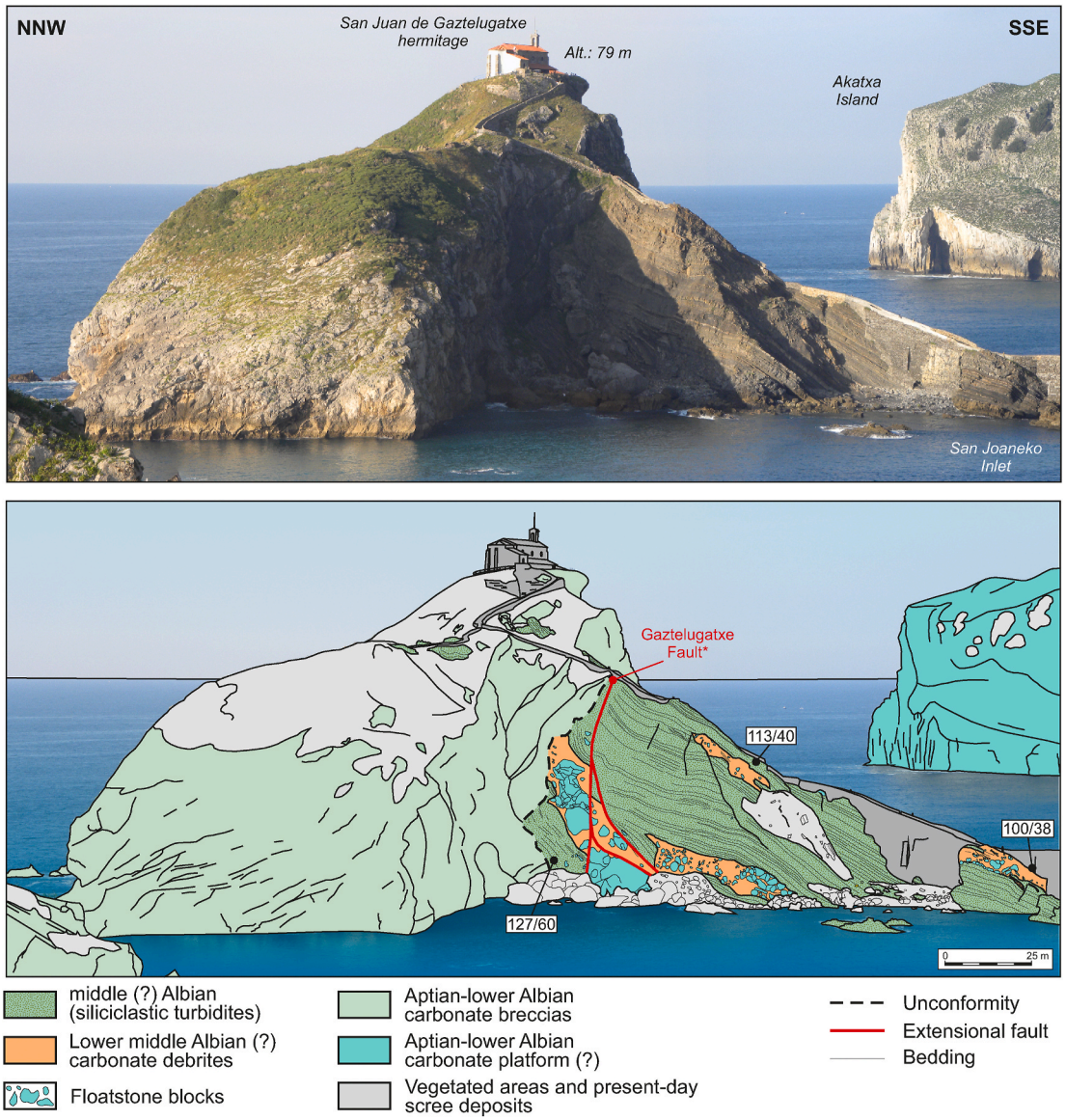

Fig. 13. Photograph looking NE with interpretation of San Juan de Gaztelugatxe peninsula showing the Aptian-lower Albian carbonate platform debrites (breccias) and the halokinetic architecture of the onlapping middle Albian successions. Numbers inside white rectangles: turbidite bedding attitudes (dip azimuth/dip); *: secondary fault according Poprawski et al. (2014).

the roof of the incipient Bakio Diapir as the salt rose with respect to the adjacent Jata-Gorliz Minibasin.

6.2. The intra-Aptian Unconformity (Ap.U.)

Close to the western diapir edge, both the overturned flap of Neocomian rocks and the growth wedge of lower Aptian marlstones are capped by a local angular unconformity (Figs. 10A and A of the supplementary data). It has a high angle of truncation (70-80°) but grades rapidly into a correlative conformity within 150–300 m of the diapir edge. It is overlain by steeply dipping (80-85°) Aptian marlstones that are parallel to this contact, which was thus folded after its formation. Part of this folding occurred during the Aptian-middle Albian, but tightening of the fold continued after the deposition of the upper Albian-lower Cenomanian turbidite/gravity-flow succession, as indicated by geometrical relationships between units and dip data on this flank of the diapir (Figs. 4 and A of the supplementary data).

6.3. Halokinetic architecture of the upper Aptian-middle Albian package

Above the intra-Aptian Unconformity on the NW diapir flank, the overlying Aptian to middle Albian deposits are in direct contact with the Bakio Diapir and comprise several stacked unconformity-bound units in which the bedding is parallel to or forming a low angle with adjacent strata or the salt interface (Fig. A of the supplementary data). The architecture of these sequences is well defined in the upper carbonate succession visible on the coastal cliffs west of the Bakio beach (Fig. 11). There, the marlstones, debrites, and turbidites of these successions display several discrete sedimentary packages that:

- are bounded by local (>200–600 m wide) angular unconformities whose truncation angles do not exceed 10-20°;
- contain a broad halo (350–400 m) of upturned beds that onlap the basal unconformities toward the diapir and show a fan arrangement with a continuous axial surface that dips toward the diapir.

Hence, they show the typical architecture of wedge HS that are

stacked to form a tapered CHS (Giles et al., 2004; Giles and Rowan, 2012).

On the other, SE diapir flank, the halokinetic architecture of this upper Aptian-middle Albian package is not so obvious, even on the coastal cliffs of the eastern diapir flank where the outcrop quality is also very high. The only easily recognizable unconformity is located at the eastern end of the Bakio beach very close to the diapir edge (Fig. A of supplementary data and Fig. 4 of Poprawski et al., 2014). This is a vertical to overturned, low-angle (<20°) unconformity that separates the marlstones and marly limestones of the lower carbonate succession from massive breccias of the upper carbonate succession. North-eastwards, the cliffs display the upper carbonate succession that comprises much thicker and continuous massive carbonate breccias in which it is very difficult to observe any internal architecture (Fig. 4), and specifically any clear unconformities that define halokinetic sequences. However, the strata form a 300–350 m broad halo of upturned bedding compared to the regional dip attitude in the eastern diapir side (20-30°; Fig. 4 and A of the supplementary data), i.e., a monocline geometry with a width and a progressive outward decrease of the bedding dip that fit the description of tapered CHS (Giles and Rowan, 2012).

The same argument can be applied for the inland part of the diapir flanks, south of the coastal cliffs, where the upper Aptian-middle Albian sediments are only visible in a few, small and isolated outcrops that rarely are in contact with the salt. Here, we recognize that: 1) there are no clear high-angle unconformities; and 2) bedding is roughly parallel to the diapir edge with dips that decrease from 70° overturned near the diapir to 60-65° (right-side-up) 270–400 m from its edge (Fig. A of the supplementary data). They too are compatible with a tapered CHS architecture.

Although the upper Aptian-middle Albian package everywhere forms a tapered CHS regardless of the stratigraphy/lithology, the internal architecture of the wedges differs along the length of the salt wall. Whereas in the central and southern parts of the salt wall, the wedges contain massive marlstones (Figs. 4 and 10A), in the northern parts, they include widespread debrites that are significantly more abundant on the eastern flank (Figs. 4 and 10A to 13). These debrites, breccias, and slumps derived from the Bakio Diapir roof (Ferrer et al., 2014; Poprawski et al., 2014), which is possibly still preserved in the inaccessible Akatxa Island (Figs. 4 and 12). Although the diapir roof can not be analyzed directly, its nature can be deciphered from the debrites clast composition and the diapir roof segments preserved at the neighboring Gernika Diapir (i.e., in the town of Mundaka; Fig. 4). In agreement with previous studies (García-Mondejar and Robador, 1987; Robles et al., 1988; Ferrer et al., 2014; Poprawski et al., 2016), these data show that, during late Aptian-early Albian times, the northern part of the Bakio Diapir roof was composed of an unlithified to lithified carbonate platform with isolated buildups at its margins.

Along neither diapir edge do the debrites contain Jurassic or Neocomian clasts. Nor are there any Upper Triassic ophite clasts in the debrites (even though they are very abundant in the outcropping salt). Thus, neither the diapir nor the oldest possible roof were involved in the mass-transport processes, and the failure surfaces/detachments of the rock falls, debris flows, and slumps were located within or at the base of the Aptian-lower Albian succession.

6.4. The Upper Albian Unconformity (U.A.U.)

The tapered CHS of the carbonate succession is topped by the widespread Upper Albian Unconformity (Fig. 4). In the Bakio area, this unconformity dips away from the salt inflated areas with an angle that diminishes gradually from up to 30° to practically horizontal in the Sollube and Jata-Gorliz minibasins (Fig. 5). Moreover, it truncates underlying rocks with an angle that decreases from near 80° at the diapir margins to practically null (<5°) at minibasin depocenters (Figs. 5 and 12 and A of the supplementary data).

The truncated rocks beneath the unconformity are progressively older not only towards the diapir edges but also to the S and SE. Thus, in the northern parts of the diapir, the U.A.U. bevels the turbidites and debrites of the upper part of the upper carbonate succession (Punta Bakio unit of Robles et al., 1988), whereas southwards, it first truncates deposits of the middle and lower part of this succession (Bermeo marls and Bakio breccias of García-Mondejar and Robador, 1987) and finally, at the southern end of the diapir, Neocomian rocks (Fig. 4 and A of the supplementary data). This trend is also present at the northern parts of the Gernika Diapir (Fig. 4) and shows that the diapir overburden was tilted towards the N-NW at the time of the formation of the U.A.U. Tilting had ceased by the end of the truncation as shown by the same age of overlying sediments around the entire diapir.

The strata above the unconformity are coarse-grained siliciclastic turbidities of the upper Albian-lower Cenomanian siliciclastic succession that both onlap or show apparent downlap onto the erosional surface. The onlaps are the predominant termination and are directed towards the inflated salt structures (Figs. 5 and 12). They develop on all diapir flanks and in the entire Sollube Minibasin (Fig. 4). The downlaps are restricted to the Jata-Gorliz Minibasin where the whole succession of turbidites dips with a 10° to 35° westward component over the near horizontal Upper Albian Unconformity (Fig. 5). The apparently downlapping layers do not have the geometry of prograding clinoforms but that of parallel beds. Thus, they indicate near-horizontal deposition and onlap of an east-dipping unconformity that was tilted westwards after the deposition of the lower Cenomanian turbidites (age of the youngest tilted rocks; Fig. 4).

6.5. Halokinetic architecture of the upper Albian (-lower Cenomanian) package

The halokinetic architecture of this succession is difficult to determine since it only appears adjacent to the diapir south of Bakio village (Figs. 4 and 10B) where it consists of dispersed small outcrops separated by highly vegetated areas. Nevertheless, the 180 bedding attitude data collected in this area reveal that above the Upper Albian Unconformity the bedding: 1) decreases in dip very gradually towards the Sollube Minibasin, from 35 to 50° at the diapir edge to 8-12° 900–1000 m basinwards (Fig. A of the supplementary data); and 2) does not change abruptly in the juxtaposed turbidite layers/units. Both observations indicate that, at this diapir flank, the upper Albian is drape folded across a broad area without internal high-angle unconformities. This rules out the existence of upper Albian hook HS and suggests that the architecture was either parallel-bedded or formed by wedge halokinetic sequences bounded by unconformities with low truncation angles (<10-15°).

In any case, the geometry indicates that the sedimentation rate in this interval was greater than the diapir uplift rate (Rowan et al., 2003). This is compatible with the siliciclastic turbidites overlapping and covering the diapir above the U.A.U. along the SE flank of the diapir (Fig. 4). Unfortunately, the original extent of this relationship is unknown due to the recent erosion that has deeply incised the central diapir areas.

7. The Bakio Diapir evolution

7.1. Pre- and synrift evolution

As shown in the previous sections, the surface data provide a good record of passive growth of the Bakio Diapir during late Aptian-late Albian times, but not of the earlier history of the diapir. This must be derived from the small and isolated outcrops of Neocomian and lower Aptian strata at the SW flank of the Bakio Diapir and mostly from the interpretation of the BR85-25 and BR85-26 seismic profiles. The combined profile (Fig. 5) shows a relatively thin Jurassic with a rather constant thickness at the base of the two minibasins, similar to the thickness observed, at the surface, next to the Gernika Diapir (~300–400 m; Soler and Solé, 1972; Boess, 1984). Similarly, the Neocomian has a mostly constant thickness, except close to the eastern edge

of the Bakio Diapir where it seems to be thicker. Thus, the Jurassic and Neocomian were pre-diapiric and that the Bakio Diapir developed later. Specifically, the salt inflation started during the early Aptian, as shown by the growth geometry of the exposed lower part of the Aptian-lower middle Albian succession at the southwestern edge of the diapir (Fig. 4 and A of the supplementary data). This geometry denotes uplift and folding of the pre-kinematic layers (Neocomian) at the future position of the diapir.

The timing of initial salt inflation coincides with activity on the pervasive system of high-angle salt-detached extensional faults that affect the older suprasalt rocks (Fig. 5), thereby implying that it was related to local overburden thinning generated by an extensional fault. The geometry and displacement of this fault are not constrained by the available data, but the lack of Jurassic in the outcropping western upturned prekinematic panel (Fig. 4) suggests that there was a gap caused by a thin-skinned extensional fault (Fig. 14). We infer this was east-dipping, accommodating thickening of the Neocomian on the eastern side of the diapir (interpretation done in Figs. 5 and 14). In this scenario, the extension and subsequent upturn of the prekinematic layers at the western diapir edge would mark reactive and active stages, respectively, of the Bakio Diapir. Moreover, the intra-Aptian unconformity (Ap.U.) indicates the time of salt breakthrough to the surface (Fig. 14).

After this initial diapir development, the tapered halokinetic architecture of the exposed successions placed over the Ap.U. (see sections 6.3 to 6.5.) show that the salt wall grew passively from the middle part of the deposition of the Aptian-middle Albian carbonate unit (Fig. 14), much earlier than proposed by Poprawski et al. (2014) who placed it at the middle Albian during the deposition of the Punta Bakio unit (uppermost part of our upper carbonate succession). As shown in Fig. 5, the onset of passive diapirism appears to be when most of the high-angle salt-detached extensional faults within the minibasins ceased to move (Fig. 5). Because salt is weaker than the cover rocks, once it pierces the suprasalt successions it absorbs any ongoing salt-detached deformation. In this case, the Bakio Diapir would have widened (cryptic extension), leading to cessation of most pre-existent thin-skinned extensional faults (Vendeville and Jackson, 1992; Jackson and Hudec, 2017).

The duration of the ongoing passive growth of the Bakio Diapir is unknown since there are no undeformed post-diapiric deposits burying it. Passive growth persisted at least into the early Cenomanian, since lower Cenomanian turbidites, although lacking clear halokinetic sequences, depict paleocurrent directions and facies architecture that indicates ongoing uplift of the diapir (see section 8 below). In any case, the halokinetic architecture of the upper Aptian-middle Albian deposits denotes that the passive growth of the diapir was accompanied by the development of wedge HS and a tapered CHS (Fig. 14). These sequences were governed, first, by the aggradation of a carbonate platform on the diapir top during late Aptian-early Albian times (Ferrer et al., 2014; Poprawski et al., 2014), and then by an increase of terrigenous input (middle Albian).

The evolution of the Bakio Diapir is interpreted to have taken place within a thick-skinned extensional tectonic setting in which (as seen on the restoration of the cross section of Fig. 3):

- the salt draped over deep active basement-involved faults.
- the diapir formed over the footwall of a major intrabasinal basement fault, probably at a thin-skinned extensional fault.
- the diapir and salt-decoupled overburden moved basinward forming a suprasalt hanging-wall ramp and, basinwards, a ramp-syncline basin generating the shifting depocenters of the Lower Cretaceous synrift succession.

In this framework, the Lower Cretaceous thickness variations (Fig. 3) as well as the geometry of the Upper Albian Unconformity with the overlying upper Albian deposits progressively truncating older strata to the South (Fig. 4) reveals that the Bakio Diapir grew during two different tectonic stages (Fig. 15).

The first, Neocomian-middle Albian in age, was coeval with extension on the basement-involved faults and overlying salt décollement. The diapir: 1) formed in a thin-skinned extensional setting just south of the hanging-wall cutoff of the Jurassic, in the footwall of the inferred Armintza-Bermeo basement fault system (Fig. 15B); and 2) was translated basinwards along the salt décollement, leading to folding and tilting of the diapir and flanking strata when they crossed over the Armintza-Bermeo basement fault (Fig. 15C to D). In this setting, it was likely that the diapir widened somewhat by extension.

The second stage, late Albian-early Cenomanian in age, was defined by the end of both tilting and fault-related thickness variations of the overburden (Fig. 15E). Hence, it is a scenario in which both the Armintza-Bermeo basement fault and the overlying salt décollement became inactive. This, together with the lack of extensional faults affecting the upper Albian successions around the salt wall, suggests that this was a period in which diapir growth was essentially governed by differential loading. The transition between the two stages is marked by the regional Upper Albian Unconformity, and was possibly related to regional uplift and the shift from crustal hyperextension to mantle exhumation as the Basque-Cantabrian Basin continued to widen (Rowan, 2014).

7.2. *Syn-Pyrenean contractional evolution*

During the late Santonian (Upper Cretaceous) to Cenozoic contractional building of the Pyrenees, the diapir was partially squeezed, as shown by the anticlines at its SSW and NNE ends (Fig. 4). Also, it was passively transported about 10 km northwards by the North Pyrenean thin-skinned thrust system (Figs. 3 and 15F). This thrust system was detached on the Upper Triassic salt layer which, at the onset of the contractional deformation, was not flat but had a complex geometry with flats and ramps resulting from the extensional motion of Upper Jurassic-Lower Cretaceous basement faults (see restoration to the end Cretaceous in Fig. 3). Therefore, during the contractional translation, diapirs and minibasins experienced changes in their original attitudes due to fault-bend folding over both frontal and lateral/oblique ramps. These latter features are not apparent at the Bakio Diapir but one is interpreted to its west. Here, the post-stretching upper Albian-Cenomanian successions filling the Jata-Gorliz Minibasin show a general dip towards the west (Fig. 4). If we restore these strata to horizontal, then (based on observations of BR85-25 seismic reflector geometry; Fig. 5) the Upper Albian Unconformity and underlying strata would have dipped to the east. This tilting, first to the east and then back to the west, may have developed by initial (southern) extensional translation and then northern (contractional) translation over a lateral ramp in the basement fault array.

8. Diapiric influence on synkinematic deposition

The passive growth of diapirs in marine environments induces seafloor highs and lows, which modify both detrital sediment flows and carbonate production, and thus the geometry and facies distribution of turbiditic fan systems (Kneller and McCaffrey, 1995; Rowan and Weimer, 1998; Toniolo et al., 2006; Mayall et al., 2010; Oluboyo et al., 2014; Nelson et al., 2018; Doughty-Jones et al., 2019; Cumberpatch et al., 2020) or carbonate platforms (Bosence, 2005; Giles et al., 2008; Esestime et al., 2015; Teixell et al., 2017; Hattori et al., 2019; Grant et al., 2019). The Bakio Diapir was a good example during its passive growth, modifying the facies arrangement at the northern margin of the Basque-Cantabrian Basin during both the latest Jurassic to middle Albian stretching/thinning stage and the late Albian to Cenomanian stage in which there was mantle exhumation and the local faults became inactive.

The first stage, during motion on the high-angle basement faults of the northern margin of the Basque-Cantabrian Basin, was characterized

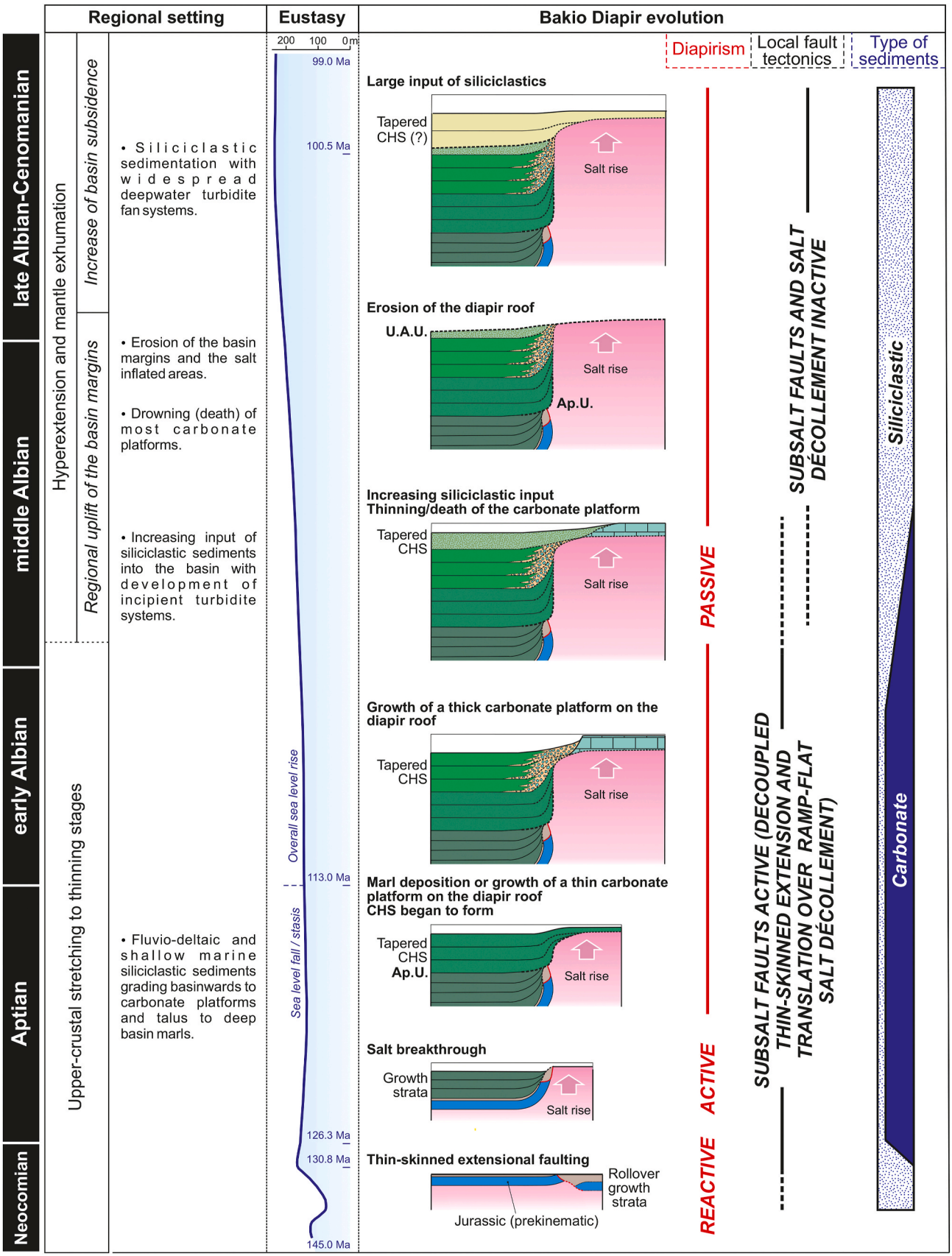

Fig. 14. Schematic cross sections showing the evolution of the Bakio Diapir from Neocomian to late Albian times and its relationship with the main sedimentary and tectonic events occurring in the Basque-Cantabrian Basin. The cross sections depict the main features of the halokinetic-sequence architecture in each evolutionary stage. Cretaceous eustasy curve from Haq (2014). Note that the stages are not in a vertical time scale (the vertical scale of the ensemble of the Albian to Cenomanian stages is nearly three times that of the Neocomian-Aptian stage).

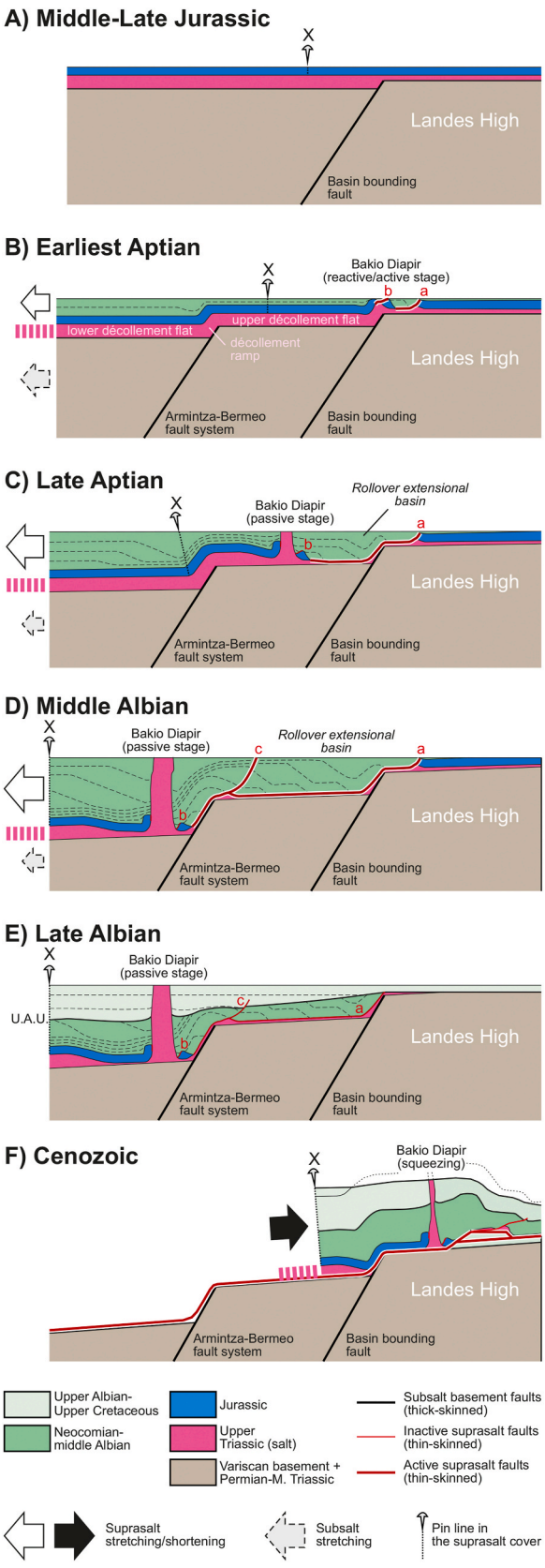

Fig. 15. Semi-quantitative sequential development of the northern margin of the Basque-Cantabrian Basin illustrating the proposed kinematic relationships between the motion of the basement faults and the kinematics of the Bakio Diapir. These sections are not precise restorations of the cross section of Fig. 3.

regionally by fluvio-deltaic and shallow marine siliciclastic deposits that graded rapidly basinwards to platform limestones and slope marlstones (Rat, 1959; García-Mondejar, 1989). This large-scale distribution of facies, however, was not simply linear and parallel to the basin margin, but was modified by both intrabasinal faults and the growth of diapirs (Robles et al., 1988). Thus, as shown by the areal distribution of the Aptian-lower Albian platform breccia clasts in the study area (Fig. 4), the carbonate platforms were not aligned along a continuous strip parallel to the northern edge of the Basque-Cantabrian Basin. Instead, they had a complex planform with salients and isolated banks that were flanked by muddy to marly depositional areas (Fig. 16). This intrincate paleogeography appears to have been largely controlled by the salt highs in anomalous basinwards positions, where carbonate buildups could grow, and intervening lows (minibasins), which were filled by muddy to marly successions. These finer-grained sediments, deposited in slope to deepwater environments (García-Mondejar and Robador, 1987), were, however, not confined to the topographic lows. They also blanketed salt highs located in more basinward positions, which did not reach a sufficient bathymetric elevation to allow the growth of carbonate buildups (i.e., the SSW end of the Bakio Diapir; Fig. 16).

The topographic control was even more evident during upper Albian to Cenomanian siliciclastic sedimentation. At that time, as noted by Vicente-Bravo and Robles (1991a), the Bakio, Bermeo, and Mungia diapirs acted as effective barriers for gravity flows and influenced the distribution of three major turbidite fan systems, each restricted to a specific minibasin (see also Cumberpatch et al., 2020). As shown by new and previously published paleocurrent data (Robador and García--Mondejar, 1987; Robles et al., 1988; Vicente Bravo and Robles, 1991a; Ábalos and Elorza, 2012; Poprawski et al., 2014; Cumberpatch et al., 2020) and mapped lateral changes in the turbidite facies (Fig. 17), relative salt rise generated sediment shadows downstream of some diapirs, where fine-grained turbidites were deposited (i.e., south of the Bermeo Diapir). Moreover, saddles, such as that located off the southern tip of the Bakio Diapir, acted as minibasin entry points, generating depletive flows that led to the accumulation downstream of coarser grained sands and even microconglomerates (eastern side of the Jata-Gorliz Minibasin).

9. Discussion

In the following discussion, we first compare and contrast our halokinetic sequence stratigraphic analysis of Bakio Diapir to that of Poprawski et al. (2014, 2016). We follow with an assessment of the factors controlling the development of tabular or tapered CHS, comparing the results of our study of the Bakio Diapir to the published models derived from predominantly shallow-water siliciclastic settings. We finish with addressing the impact of the major intra-Albian shift in rift style on the growth of passive diapirs in the Basque-Cantabrian Basin.

9.1. CHS at Bakio Diapir

Our observations at Bakio Diapir show that Aptian through Albian passive growth was accompanied by the formation of a series of tapered CHS (Fig. 14), which is consistent with the Poprawski et al. (2014, 2016) analysis of the Bakio breccia succession, but inconsistent with their analysis of the underlying Aptian-lower Albian Bakio marlstones. The latter are bounded at the top by their halokinetic-sequence bounding angular unconformity u1. Based on the angularity of this unconformity (40°) on the eastern side of Bakio Diapir, they interpret the marlstones underlying the Bakio breccias to form a hook HS and infer it was part of a stack of hook HS forming a tabular CHS. They further suggest that the marlstones were deposited in a period of time of slow sedimentation rates prior to major influx of turbidites derived from the Landes Massif to the north, and that Bakio Diapir passive-rise rates outpaced sediment-accumulation rates, thereby generating a tabular CHS. We

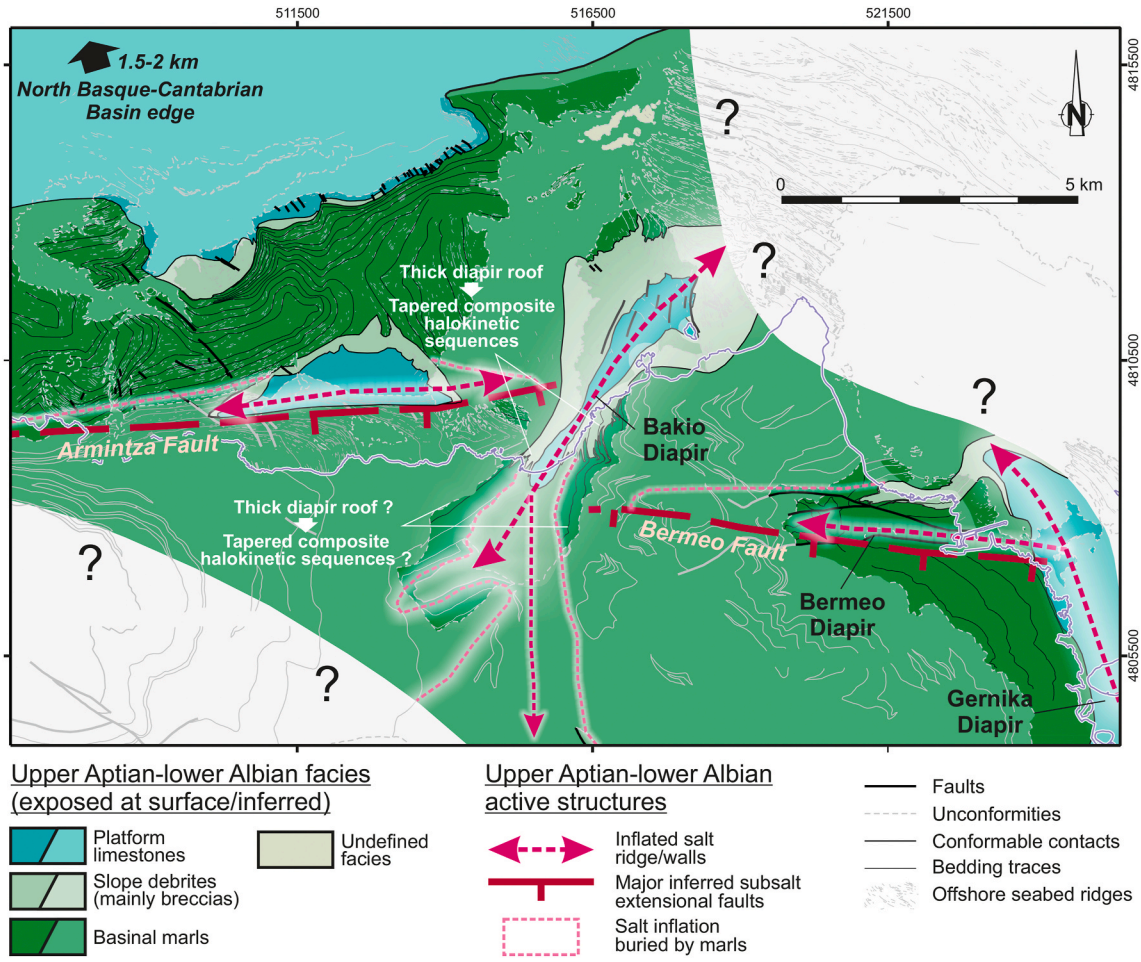

Fig. 16. Facies architecture of the upper Aptian-middle Albian carbonate-dominated succession showing its relationship with the inferred diapirism and thin-skinned extension. The map area is the same as in Fig. 4 and the right column of the legend shows structures of the present-day geologic map. Note that the Aptian-lower Albian salt and fault features would have been about 13 km to the south prior to Pyrenean thrusting.

interpret the same angularity as reflecting that expected by the oldest wedges in a tapered CHS juxtaposed across the angular unconformity with the overlying Bakio Breccias Fm. (see Fig. 1B, bottom). We do not recognize any tabular CHS at Bakio Diapir, and the width of the deformation halo (zone of halokinetic drape folding flanking a diapir) shows that the marlstones instead form a tapered CHS.

Poprawski et al. (2016) interpret the Bakio Breccia Fm. (our upper carbonate succession) as basinal mass wasting and turbidites shed into the adjacent minibasin from carbonate platforms developed on diapir bathymetric highs. The carbonate platforms rapidly aggrade and build up relief over the diapir during transgression and naturally shed abundant carbonate debris down the escarpment into the basin. The high rates of sediment accumulation produce a thick roof over the diapir resulting in wedge HS and tapered CHS. They highlight that carbonate halokinetic sequences, either wedges or hooks, may contain abundant gravity flows, which sets them apart from their siliciclastic counterparts. Our interpretation is fundamentally the same. However, they interpret that platform aggradation at Bakio took place during the transgressive systems tracts of depositional sequences and that no highstand systems tracts or lowstand systems tracts sediments are preserved. We do not relate these strata to depositional sequences and eustastic sea level cycles, but interpret the system as long-term progressive deepening across the Bakio Diapir area driven primarily by translation over the ramp in the detachment, tectonic subsidence, and eustatic sea-level rise (see discussion below).

9.2. *Controlling factors on CHS development*

Defined in shelf settings (Giles and Rowan, 2012), tapered and tabular CHS are distinguished based on their geometric attributes, but are further interpreted to vary in: 1) ratios between the local sediment-accumulation rate and the salt-rise rate; 2) the consequent thickness of the roof; 3) the height and steepness of the topograpic relief above the edge of salt; and 4) the resultant presence or absence of associated debrites or other reworked sediment derived from the roof or diapir. We address these in turn below, in all cases ultimately attributing the differences between the Bakio Diapir and the established models to the development of a carbonate platform on top of the Bakio Diapir (Rowan et al., 2012b).

9.2.1. *Relative sediment-accumulation rates*

Tabular and tapered CHS normally form when the ratio between sediment-accumulation and salt-rise rates is low or high, respectively. For a given salt-rise rate, therefore, tabular and tapered CHS suggest relatively slow and fast sediment accumulation rates, respectively. This is consistent with our observations in the middle Albian to lower Cenomanian halokinetic successions of the Bakio Diapir, where the presumed fast overall regional sedimentation rate of the siliciclastic gravity flows derived from the uplift of the Landes Massif was accompanied by the formation of tapered CHS (Fig. 14). However, it does not match the sedimentary signature of the underlying carbonate Aptian-lower Albian successions. The regional marly Aptian-lower Albian infill of the minibasins, with a supposed low regional sedimentation rate, did not lead to

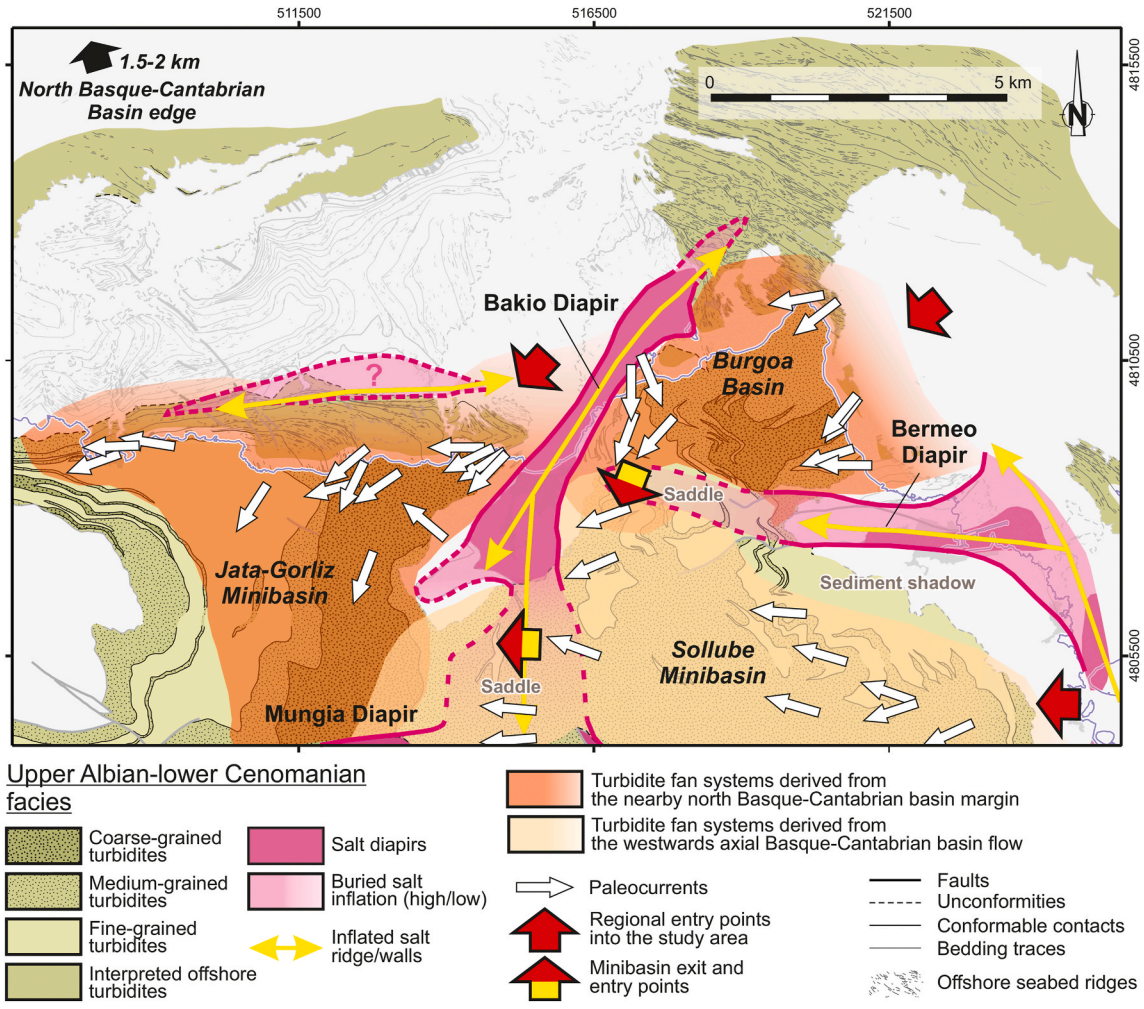

Fig. 17. Facies architecture of the upper Albian-lower Cenomanian succession showing its relationships with the growing salt diapirs. The map area is the same as in Fig. 4 and the right column of the legend shows the primary and secondary structures of the present-day geologic map. The represented turbidite facies belts are bounded by the present-day surface contacts which are heterochronous; thus, the map does not reproduce a specific late Albian-early Cenomanian time span because the turbiditic bodies changed their areal distribution over time (Cumberpatch et al., 2020). Also note that the upper Albian-lower Cenomanian salt structures would have been about 13 km to the south prior to Pyrenean thrusting (see Figs. 2 and 7). Paleocurrent data compiled from Robador and García-Mondejar (1987), Robles et al. (1988), Vicente Bravo and Robles (1991a), Ábalos and Elorza (2012), Poprawski et al. (2014), and our study.

generation of tabular CHS but was accompanied by the formation of a tapered CHS (Figs. 11 and 16, and A of the supplementary data). Our explanation lies in the difference in depositional rates between minibasins and diapir roofs (Fig. 18): in siliciclastic systems, sediment accumulation is slower above the topographic highs of diapirs, comprising thin, condensed muddy facies (e.g., Johnson and Bredeson, 1971; Moore et al., 1995). In contrast, if water depths are shallow enough and the paleoecological conditions are suitable, carbonate platform growth is more rapid (e.g., Pomar and Ward, 1995; Moore and Wade, 2013) than coeval marly deposition in the minibasins. Thus, it is not enough to look only at the regional sediment-accumulation rate. HS and CHS types are dependent on the local sediment-accumulation rate on the roof and flanks relative to the rate of rise of the diapir underlying that roof.

9.2.2. *Roof thickness*

The ultimate control on the width of the deformation halo, and thus the development of tabular or tapered CHS, is the thickness of the roof (Giles and Rowan, 2012; Hearon et al., 2014; Rowan et al., 2020). Roof thickness determines the wavelength of the drape fold, that is the width of the folded area of each halokinetic sequence. Thus, thin roofs generate narrow tilted panels (tabular CHS) and thick roofs generate wide monoclinal fold limbs (tapered CHS). In terrigenous to mixed depositional environments, again, roof thickness is controlled by the ratio between salt-rise and local sediment-deposition rates (Giles and Rowan, 2012), although variable roof erosion can play a role (Hearon et al., 2014). However, carbonate buildups above diapirs, as occurred in the northern parts of the Bakio Diapir (Poprawski et al., 2016), tend to generate thick roofs and thus tapered CHS regardless of the regional deposition rate.

Growth of a carbonate platform above a diapir does not however necessarily imply the development of tapered CHS (Giles et al., 2008). It depends on the interplay between the rates of diapir roof uplift and the subsidence of the subsalt rocks beneath the diapir and minibasins, which can be regional and/or due to local deformations (i.e., subsalt faulting or folding). Thus, disregarding the effect of sea-level variations, if the uplift of the diapir roof is greater than subsalt subsidence, the vertical accommodation space for the carbonate platform to develop will reduce with time (Fig. 19A). The platform will be eroded and, as a result, the progressively thinner roof will favor the development of tabular CHS. On the other hand, if the diapir roof uplift is slower than the subsidence, the accommodation space will increase and the platform will thicken by aggradation. Thus, thick diapir roofs will develop, thereby leading to the formation of tapered CHS (Fig. 19B).

	Feature	Diapir roof with dominantly siliciclastic sediments	Diapir roof made by a vertically aggrading carbonate platform
Wedge HS / Tapered CHS	Roof thickness	Thick	Thick
	Topographic relief	Low	**Rather high**
	Width of drape folding	300-1000 m	300-1000 m
	HS angular unconformities	Up to 30°	Up to 30°
	Facies changes in the halokinetic sequences	Broad zone of gradational facies changes with few debrites	Broad zone **with some abrupt facies changes and abundant debrites**
	Sedimentary aggradation rate at the diapir roof and edges	Rather high	**High**
	Sedimentation rate at the adjoining minibasins	High	**Not necessarily high**
	Ratio between the diapir rise and sedimentation rates on diapir top	Low	Low
	Ratio between the sedimentation rates on diapir top and in adjacent minibasins	<1	**>1**

	Feature	Diapir roof with siliciclastic or mixed sediments	Diapir roof made by an eroding carbonate platform
Hook HS / Tabular CHS	Roof thickness	Thin	**Progressively thinner (thin)**
	Topographic relief	High	**Decreasing**
	Width of drape folding	50-200 m	50-200 m
	HS angular unconformities	Up to 90°	Up to 90°
	Facies changes in the halokinetic sequences	Narrow zone with abrupt facies changes and debrites close the diapir edge	Narrow zone with abrupt facies changes and debrites close the diapir edge
	Sedimentary aggradation rate at the diapir roof and edges	Low	**Null (erosion)**
	Sedimentation rate at the adjoining minibasins	Low	**Not necessarily low**
	Ratio between the diapir rise and sedimentation rates on diapir top	High	High
	Ratio between the sedimentation rates on diapir top and in adjacent minibasins	<1	**Decreasing (<1)**

Fig. 18. Tables showing the similarities (black text) and differences (red text) between tapered and tabular CHS defined in dominantly siliciclastic environments (Giles and Rowan, 2012) and those characterized by a growing carbonate platform (this study). (For interpretation of the references to color in this figure legend, the reader is referred to the Web version of this article.)

In this regard, the absence, expansion, and later retraction of the carbonate platform debrites during the upper Aptian-middle Albian passive growth of the Bakio Diapir (see Fig. 10A), points to changes in the thickness of the diapir-roofing carbonate platform – that is, in the vertical accommodation space over the diapir. In particular, they denote an increase of the roof thickness/accommodation space during the late Aptian-early Albian and a progressive decrease during the middle Albian. Considering that the uplift of the diapir roof probably did not change significantly over this time interval, these variations could be related to sea level that fell through the Aptian and rose during the Albian (Haq, 2014) as well as to changes in the subsalt subsidence rates. Indeed, the restoration of the regional cross section (Fig. 15) shows that the Bakio Diapir moved over a décollement with a flat-ramp-flat geometry, which implies three evolutionary stages with a different base of salt subsidence: 1) an initial (Aptian?) phase in which the diapir moved along the upper flat, characterized by no or very little subsidence of the diapir base (stages B and C of Fig. 15); 2) an intermediate stage (early Albian?) in which translation of the Bakio Diapir down the ramp resulted in a significant increase in diapir base subsidence (between Fig. 15C and D); and 3) a last stage (middle Albian?) similar to the first, in which translation along the lower flat again resulted in little to no base-salt subsidence (stage D in Fig. 15).

Conversely, aggradation of a carbonate platform above the Bakio diapir roof cannot be invoked to explain the tapered architecture of either the lower carbonate succession or the upper carbonate succession in the southern parts of the diapir. In both cases there are no carbonate platform debrites indicating the presence of an aggrading carbonate platform above the diapir (see above and Figs. 10A and 14). Instead, the architecture is typical of standard tapered CHS (Giles and Rowan, 2012), implying that the aggradation rate of the marls exceeded the diapir-rise rate.

9.2.3. *Topographic relief*

The established models hold that tabular CHS have high, steep scarps above diapir edges, whereas tapered CHS have lower and gentler relief (Giles and Rowan, 2012). Again, though, this is based on siliciclastic systems. However, as Rowan et al. (2012b) and Poprawski et al. (2016) highlight, in carbonate environments, aggradation of carbonate platforms on top of diapirs can create steep slopes on the diapir edges even though they form tapered CHS (Figs. 18 and 19).

Sea-level fluctuations play a role in determining topographic relief in both deepwater siliciclastic systems and shallow-water carbonate systems, but in different ways. In the former, relative highstands of sea level lead to condensed, draping facies (e.g., Prather et al., 1998). Since the diapir still rises and the minibasins still sink, both the amplitude and steepness of topographic relief thus increase. They also increase in

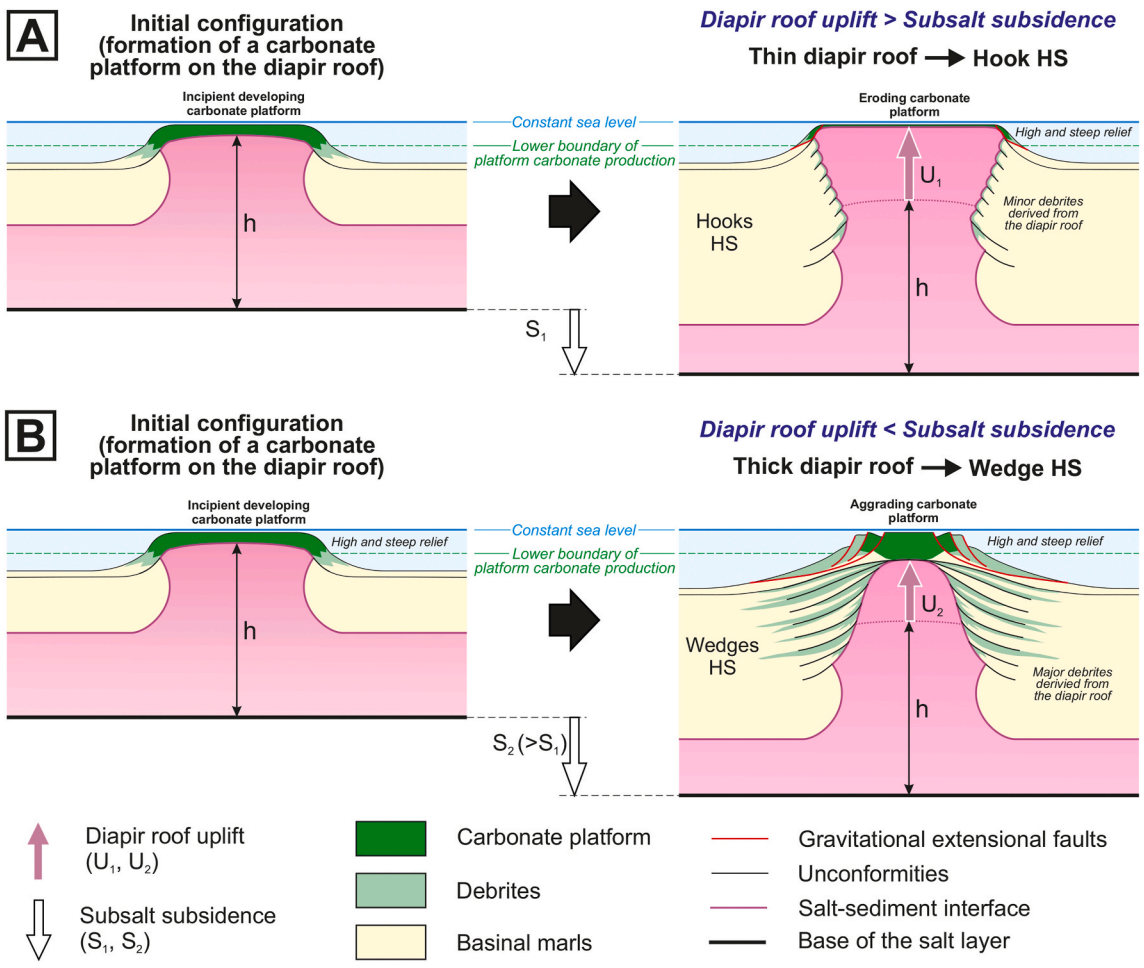

Fig. 19. Halokinetic-sequence architecture of passive diapirs developed in a carbonate environment characterized by the deposition of platform limestones on the diapir roof and marlstones in the adjacent minibasins. **A)** Model with diapir uplift rate higher than the subsidence rate (regional or locally fault/fold related) of the underlying substratum (subsalt subsidence). **B)** Model with diapir uplift rate lower than the subsalt subsidence rate. Note that in both cases, the applied marly sedimentation rate in minibasins is the same. h: Diapir height in the first depicted stage (left).

shallow-water carbonate systems, but in this case driven more by vertical aggradation of platforms that keep pace with the rising sea level as the minibasins sink.

9.2.4. *Reworked sediment*

In tapered CHS in siliciclastic systems, because they are characterized by low and gentle relief, slumped and otherwise reworked sediment is rare to absent (Giles and Rowan, 2012). In the case of carbonate platforms and specifically the Bakio Diapir, however, the thick roofs and steep scarps generated a large amount of reworked sediment, in the form of debrites and calcarenites, down the topographic slope (Rowan et al., 2012b; Poprawski et al., 2016). These combined to increase the roof thickness at the diapir edge and reduce the topographic slopes, two responses that helped drive the formation of halokinetic sequences with broad and gentle drape-fold geometries that were bounded by low-angle truncational unconformities.

Our study emphasizes that debrites are not exclusive to hook HS and tabular CHS as postulated in siliciclastic environments (Rowan et al., 2003; Giles et al., 2004; Giles and Rowan, 2012). This means that in wedge HS developed in carbonate environments: a) the sediments derived from slope collapse (debrites, slumps, etc.) can be rather abundant (Figs. 18 and 19B), and b) some of the halokinetic-sequence bounding unconformities are linked to the failure scarps. Moreover, whereas in terrigenous to mixed environments, halokinetic-sequence boundaries and overlying debrites are linked to sea level fluctuations and the times of slowest sedimentation (Giles and Rowan, 2012; Hearon et al., 2014; Mianaekere and Adam, 2020), the high relief of carbonate platforms may generate collapse, and thus debrites and unconformities, more frequent and at any time. In this sense, the depositional environment appears to be a key factor determining not only the roof thickness and therefore the type of halokinetic sequence (hook or wedge), but also its stratigraphic extent and internal character.

9.2.5. *The Bakio Diapir*

Keeping in mind the analysis of controlling factors on halokinetic-sequence development, we deduce the following for the Bakio Diapir during Aptian-early Albian times:

First, the sedimentation rate of the Aptian-lower Albian marls was not as low as suspected but rapid enough to compensate and even exceed the diapir uplift rate, thereby generating a tapered CHS. The uplift rate was probably rather slow at first because the total minibasin infill was still relatively thin and thus the differential load was not large, but might have increased considerably during ongoing deposition and consequent minibasin thickening.

Second, during the deposition of the upper carbonate succession (latest Aptian?-middle Albian), the top of the diapir was deeper in the south than in the north, where it was shallow enough to allow development of a carbonate platform.

And finally, the accommodation space for sediment aggradation on top of the Bakio Diapir increased, at least in the north and during the early Albian, more quickly than the diapir rose, allowing the formation of a relatively thick carbonate platform and, consequently, a tapered

CHS. We suggest that this accommodation space increase was related to the Albian progressive rise of sea level (Haq, 2014) but also to a greater subsidence of the base of the Bakio Diapir induced by the south-directed translation of the diapir over and down the décollement ramp developed over the active subsalt Armitza-Bermeo fault system (Fig. 15).

9.3. Impact of rift evolution on passive diapir growth

As summarized earlier, the transition from the middle to late Albian marked a period of lithospheric uplift of the rift margins, possibly due to upwelling of asthenospheric mantle, which in turn led to the development of a widespread erosive unconformity and a large input of terrigenous sediments to the still subsiding basinal areas (Jammes et al., 2010; Masini et al., 2014; DeFelipe et al., 2017; Muñoz, 2019). This has been linked regionally to the shift from crustal thinning to exhumation of lithospheric mantle (e.g., Jammes et al., 2009; Rowan, 2014). Regardless of the details of crustal rifting, though, in the Bakio area this was the time when local subsalt faults and decoupled suprasalt extension ceased (Figs. 3B and 15) as further rifting shifted to more basinal (southerly) positions. Our study of the Bakio Salt Diapir and available information from other diapirs of the Basque-Cantabrian Basin and Pyrenees (e.g., Brinkmann et al., 1967; García-Mondejar, 1982; Boess, 1984; Canérot and Lenoble, 1993; Agirrezabala et al., 2002; Canérot et al., 2005; Muñoz and García-Senz, 2010; Quintà et al., 2012; Bodego and Agirrezabala, 2013; Bodego et al., 2018) suggest that these changes may have had an impact on the growth of the salt diapirs in two manners.

First, erosion of the basin margins led to the partial or total removal of the roofs of the diapiric structures located in these areas. Consequently, it might have caused an increase in salt extrusion (although this cannot be documented at the Bakio Diapir) and the development of widespread unconformities extending far away from the rising diapirs. Such unconformities would have been drape folded by ongoing diapirism and onlapped and overlain by sediments deposited during subsequent rift-related basin subsidence, as shown by the U.A.U. at the western side of the Bakio Diapir (Fig. 12).

Second, the sudden input of a large amount of siliciclastics coming from the Landes Massif (Voort, 1964; Puelles et al., 2014; Cumberpatch et al., 2020) resulted in: a) the demise of the carbonate platforms growing above the diapirs; and b) a significant increase in the sediment-accumulation rates in the minibasins, as shown in the Basque-Cantabrian Basin by subsidence and stratigraphic studies (García-Mondejar et al., 2005; López-Horgue et al., 2009). This increase would have counteracted and possibly overcome the increase in salt-rise rate generated by the erosion of the diapir roofs and the cessation of carbonate platform growth.

Many diapirs of the Basque-Cantabrian and other Pyrenean basins show prominent changes in growth style at this same stratigraphic level (e.g., Boess, 1984; Muñoz and García-Senz, 2010; Quintà et al., 2012; Saura et al., 2016; Bodego et al., 2018). These changes include narrowing of existent passive diapirs, with possible formation of diapir shoulders, and initiation of passive diapirism by erosional unroofing of precursor bodies of inflated salt. Moreover, such effects of sudden increases in sediment input and/or regional unconformities are found in many other salt basins, whether rifted basins or not. Examples of the former include the Atlas Mts., where the terrigenous Aalenian partially overlies the diapir roofs (Saura et al., 2013; Vergés et al., 2017) and the Northern Calcareous Alps, where the terrigenous middle Carnian Lunz Fm. also expands over the diapirs and forms some diapir shoulders (Granado et al., 2018). Regional unconformities have triggered the onset of passive diapirism in basins such as the Paradox Basin (Rowan et al., 2016; Escosa et al., 2018) and the Nordkapp Basin (Rowan and Lindsø, 2017), have led to shoulder formation (e.g., Paradox Basin, Giles et al., 2018), or are associated with prominent changes in salt-flank geometry (e.g., southern Gulf of Mexico, unplublished data).

10. Conclusions

The Bakio Diapir is a NNE-trending salt wall sourced from prerift Upper Triassic salt whose formation was linked to thick-skinned extension. In particular, it is interpreted as related to Aptian displacement on two slightly overlapping basement-involved faults that generated a salt-detached drape fold in which the cover was stretched and tectonically thinned triggering salt breakthrough and passive diapirism. The subsequent evolution was constrained by southwards transport of the diapir and adjoining overburden over fault-stepped basement. This continued until the late Albian, when the basement faults became inactive and corresponding suprasalt extension effectively ceased.

The diapir is flanked to the north by rollover extensional basins (i.e, Burgoa Basin) and to the east and west two bowl-shaped minibasins (Sollube and Jata-Gorliz, respectively). The depocenters were filled by sediments deposited, first, in a carbonate platform to slope environment, and then in siliciclastic deepwater fans at slope aprons. Regardless of the depositional environment, all flanking strata show tapered CHS architecture during its recorded passive growth. Most of the wedges forming these composite halokinetic sequences do not include debrites coming from the diapir roof, but there are some in which such deposits are predominant, specifically those developed on the northern part of the diapir during lower Albian carbonate deposition. The abundance of debrites was related to the aggradation of a carbonate platform above the diapir, which generated: 1) a thick diapir roof; and 2) high and steep topographic relief.

The Bakio Diapir, with such features, offers one of the few exposed opportunities for analyzing the structural and sedimentary features developed during growth of passive diapirs in deepwater environments with both synkinematic carbonate and siliciclastic strata. This outstanding natural laboratory allows us to evaluate the factors controlling the architecture and evolution of the diapir and surrounding halokinetic sequences.

- The geometry of the halokinetic sequences is defined, regardless of setting, by the thickness of the roof edges. Thus, thick diapir roofs generate wedge HS and tapered CHS, and thin diapir roofs form hook HS and tabular CHS.
- The thickness of the diapir roof is often controlled by the ratio between salt-rise and local sediment-accumulation rates but also, in carbonate environments, by the water depth of the diapir roof and the environmental conditions that can promote the aggradation of a carbonate buildup on top of the diapir. Thus, thick diapir roofs and tapered CHS can form even though the ratio was high in this case due to slow, marly deposition in the minibasins.
- The diapir roof thickness is also controlled in shallow-water carbonate settings by the accommodation space available over the top of the diapir, which itself is determined by: a) sea-level fluctuations; and b) the interplay between the uplift of diapir top and the regional/local tectonic subsidence of the diapir base.
- High and steep scarps over the edges of diapirs, and thus abundant debrites, are not exclusive to hook HS and tabular CHS. They can be also present in wedge HS and tapered CHS that formed from the aggradation of a thick carbonate buildup on top of a diapir.

Finally, our study also shows that a regional shift in the styles of lithospheric extension, which occurred in the Basque-Cantabrian Basin during the transition from the middle to late Albian, impacted diapirism by: a) cessation of local basement faulting and, therefore, the end of suprasalt stretching that widened the passive diapirs originally developed in their footwalls; b) uplift of the rift margins and erosion of the roofs of marginal diapirs, which removed or thinned the roofs, thereby possibly favoring salt extrusion; and c) a sudden input of a large amount of siliciclastics into the basin, which terminated most or even all carbonate buildups above the diapirs and thus resulted in changing halokinetic-sequence architecture.

CRediT authorship contribution statement

Eduard Roca: Conceptualization, Methodology, Investigation, Resources, Writing - original draft, Visualization. **Oriol Ferrer:** Conceptualization, Investigation, Resources. **Mark G. Rowan:** Conceptualization, Methodology, Writing - review & editing. **Josep Anton Muñoz:** Conceptualization, Methodology, Writing - review & editing. **Mireia Butillé:** Software, Investigation, Resources. **Katherine A. Giles:** Investigation, Resources, Writing - review & editing. **Pau Arbués:** Investigation, Resources. **Marco de Matteis:** Validation, Investigation, Resources.

Declaration of competing interest

The authors declare that they have no known competing financial interests or personal relationships that could have appeared to influence the work reported in this paper.

Acknowledgements

This work was funded by the projects CGL2014-54118-C2-1-R/BTE MINECO/FEDER, UE and CGL2017-85532-P AEI/FEDER, UE of the Ministerio de Economía y Competitividad, the GEOMODELS Research Institute, and the Grup de Geodinàmica i Anàlisi de Conques (2014SGR-467), and also by the industry sponsors of the Salt-Sediment Interaction Research Consortium at the University of Texas at El Paso. The authors wish to acknowledge Carl Fiduk, Simon Baker, Allen Frankovic, and Juan García Portero for helpful discussions and all the people who helped in the numerous field campaigns. Also we thank Zoë Cumberpatch and two anonymous reviewers whose comments greatly improved the manuscript. Finally, we also acknowledge Schlumberger, ParadigmMT, and Petroleum Experts (Petex) for providing the academic licenses of Petrel, GoCad, and Move software, respectively, used in the seismic interpretation, geological mapping and structural interpretation.

Appendix A. Supplementary data

Supplementary data to this article can be found online at https://doi.org/10.1016/j.marpetgeo.2020.104770.

References

Ábalos, B., 2016. Geologic map of the Basque-Cantabrian Basin and a new tectonic interpretation of the Basque Arc. Int. J. Earth Sci. 105, 2327–2354. https://doi.org/10.1007/s00531-016-1291-6.

Ábalos, B., Elorza, J., 2012. Structural diagenesis of late Albian siderite layers of the black Flysh (Armintza Bay, Basque Cantabrian Basin, N Spain). J. Geol. 120 (4), 405–429. https://doi.org/10.1086/665794.

Agirrezabala, L.M., 1996. El Aptiense-Albiense del Anticlinorio Nor-Vizcaíno entre Gernika y Azpeitia. PhD thesis. UPV/EHU, Getxo, Spain.

Agirrezabala, L.M., García-Mondejar, J., 1989. Evolución tectonosedimentaria de la plataforma urgoniana entre Cabo Ogoño e Itziar (Aptiense-Albiense superior, Región Vasco-Cantábrica Nor-oriental). Bilbao Spain. In: XII Congreso Español de Sedimentología, pp. 11–20.

Agirrezabala, L.M., Owen, H.G., García-Mondejar, J., 2002. Syntectonic deposits and punctuated limb rotation in an Albian submarine transpressional fold (Mutriku village, Basque-Cantabrian basin, northern Spain). Geol. Soc. Am. Bull. 114 (3), 281–297. https://doi.org/10.1130/0016-7606(2002)114<C0281:SDAPLR>2.0.CO,2.

Alsop, G.I., Weinberger, R., Levi, T., Marco, S., 2016. Cycles of passive versus active diapirism recorded along an exposed salt wall. J. Struct. Geol. 84, 47–67. https://doi.org/10.1016/j.jsg.2016.01.008.

Amiot, M., 1982. El Cretácico Superior de la región Navarro-Cántabra. In: García, A. (Ed.), El Cretácico de España. Editorial de la Universidad Complutense de Madrid, Madrid, pp. 88–111.

Arbués, P., Ferrer, O., Roca, E., Giles, K., Rowan, M., De Matteis, M., Muñoz, J.A., 2012. The Bakio salt wall and its effects on synkinematic deepwater sedimentation (Basque Pyrenees, Northern Spain). Vienna, Austria. In: EGU General Assembly Conference Abstracts, vol. 14, p. 9659.

Barrón, E., Peyrot, D., Rodríguez-López, J.P., Meléndez, N., López del Valle, R., Najarro, M., Rosales, I., Comas-Rengifo, M.J., 2015. Palynology of Aptian and upper Albian (Lower Cretaceous) amber-bearing outcrops of the southern margin of the Basque-Cantabrian basin (northern Spain). Cretac. Res. 52 (A), 292–312. https://doi.org/10.1016/j.cretres.2014.10.003.

Béziat, D., Joron, J.L., Monchoux, P., Treuil, M., Walgenwitz, F., 1991. Geodynamic implications of geochemical data for the Pyrenean ophites (Spain-France). Chem. Geol. 89 (3–4), 243–262. https://doi.org/10.1016/0009-2541(91)90019-N.

Bodego, A., Agirrezabala, L.M., 2013. Syn-depositional thin- and thick-skinned extensional tectonics in the mid-Cretaceous Lasarte sub-basin, western Pyrenees. Basin Res. 25 (5), 594–612. https://doi.org/10.1111/bre.12017.

Bodego, A., Iriarte, E., Agirrezabala, L.M., García-Mondejar, J., López-Horgue, M.A., 2015. Synextensional mid-Cretaceous stratigraphy architecture of the Eastern Basque-Cantabrian basin margin (western Pyrenees). Cretac. Res. 55, 229–261. https://doi.org/10.1016/j.cretres.2015.01.006.

Bodego, A., Iriarte, E., López-Horgue, M.A., Álvarez, I., 2018. Rift-margin extensional forced folds and salt tectonics in the eastern Basque-Cantabrian rift basin (western Pyrenees), 582 Mar. Petrol. Geol. 91, 667. https://doi.org/10.1016/j.marpetgeo.2018.02.007.

Boess, J.G.V., 1984. Der diapir von Gernika. Z. Dtsch. Geol. Gesell. Band 135, 7–21.

Bosence, D.W.J., 2005. A genetic classification of carbonate platforms based on their basinal and tectonic settings in the Cenozoic. Sediment. Geol. 175 (1–4), 49–72. https://doi.org/10.1016/j.sedgeo.2004.12.030.

Brinkmann, R., Lögters, H., Pflug, R., Von Stackelberg, U., Hempel, P.M., Kind, H.D., 1967. Diapir-tektonik und stratigraphie im vorland der spanischen Westpyrenäen. Beih. Geol. Jahrb. 66, 183.

Cámara, P., 2017. Salt and strike-slip tectonics as main drivers in the structural evolution of the Basque-Cantabrian Basin, Spain. In: Soto, J.I., Flinch, J.F., Tari, G. (Eds.), Permo-Triassic Salt Provinces of Europe, North Africa and the Atlantic Margins. Elsevier, Amsterdam, pp. 371–394.

Cámara, P., 2020. Inverted turtle salt anticlines in the Eastern Basque-Cantabrian basin, Spain. Mar. Petrol. Geol. 117 https://doi.org/10.1016/j.marpetgeo.2020.104358.

Canérot, J., Lenoble, J.L., 1993. Diapirisme crétacé sur la marge ibérique des Pyrénées occidentales: exemple du pic de Lauriolle; comparaisons avec l'Aquitaine, les Pyrénées centrales et orientales. Bull. Soc. Geol. Fr. 164 (5), 719–726.

Canérot, J., Hudec, A.R., Rockenbauch, K., 2005. Mesozoic diapirism in the Pyrenean orogen: salt tectonics on a transform plate boundary. AAPG Bull. 89 (2), 211–229. https://doi.org/10.1306/09170404007.

Carola, E., Muñoz, J.A., Roca, E., 2015. The transition from thick-skinned to thin-skinned tectonics in the Basque-Cantabrian Pyrenees: the Burgalesa Platform and surroundings. Int. J. Earth Sci. 104, 2215–2239. https://doi.org/10.1007/s00531-015-1177-z.

Coleman, A.J., Jackson, C.A.-L.-, Duffy, O.B., Nikolinakou, M.A., 2018. How, where, and when do radial faults grow near salt diapirs? Geology 46 (7), 655–658. https://doi.org/10.1130/G40338.1.

Counts, J.W., Dalgarno, C.R., Amos, K.J., Hasiotis, S.T., 2019. Lateral facies variability along the margin of an outcropping salt-withdrawal minibasin, South Australia, 867 28-45 J. Sediment. Res. 89 (1). https://doi.org/10.2110/jsr.2019.2.

Cumberpatch, Z.A., Kane, I.A., Soutter, E.L., Hodgson, D.M., Jackson, C.A.-L., Kilhams, B. A., Poprawski, J., 2020. Interactions of deep-water gravity flows and active salt tectonics (in review). J. Sediment. Res.. https://doi.org/10.31223/osf.io/j42ha.

DeFelipe, I., Pedreira, D., Pulgar, J.A., Iriarte, E., Mendia, M., 2017. Mantle exhumation and metamorphism in the Basque-Cantabrian Basin (N Spain): stable and clumped isotope analysis in carbonates and comparison with ophicalcites in the North-Pyrenean Zone (Urdach and Lherz). G-cubed 18 (2), 631–652. https://doi.org/10.1002/2016GC006690.

DeFelipe, I., Pulgar, J.A., Pedreira, D., 2018. Crustal structure of the eastern Basque-Cantabrian zone-western Pyrenees: from the Cretaceous hyperextension to the Cenozoic inversion. Rev. Soc. Geol. Espana 31 (2), 69–82. https://hdl.handle.net/10651/52197.

Mesozoic and Cenozoic Sequence Stratigraphy of European Basins. In: De Graciansky, P. C., Hardenbol, J., Jacquin, T., Vail, P.R. (Eds.), 1998, vol. 60. SEPM Special Publication, p. 786.

Doughty-Jones, G., Lonergan, L., Mayall, M., Dee, S.J., 2019. The role of structural growth in controlling the facies and distribution of mass transport deposits in a deep-water salt minibasin. Mar. Petrol. Geol. 104, 106–124. https://doi.org/10.1016/j.marpetgeo.2019.03.015.

Escosa, F., Rowan, M.G., Giles, K.A., Deatrick, K.T., Mast, A.M., Langford, R.P., Hearon IV, T.E., Roca, E., 2018. Lateral terminations of salt walls and megaflaps: an example from Gypsum Valley diapir, Paradox Basin, Colorado, USA. Basin Res. 31, 191–212. https://doi.org/10.1111/bre.12316.

Esestime, P., Browning-Stamp, P., Hewitt, A., 2015. Evidence of early halokinesis in the Zechtein Group suggests the formation of Permian-Triassic carbonate build-ups offshore UK (Quad. 20-21). First Break 33 (12), 69–75.

Espejo, J.A., Martínez, C., Granados, L., Saavedra, J.L., Martín, L., Fernández, M.C., Del Pan, T., Heras, A., Torres, T., 1975. Mapa Geológico de España E. 1:50.000 BERMEO. IGME, Madrid, p. 23.

Fernández-Mediola, P.A., Gómez-Pérez, I., García-Mondejar, J., 1993. Aptian-albian carbonate platforms: central Basque-Cantabrian Basin, northern Spain. In: Toni Simo, J.A., Scott, R.W., Masse, J.P. (Eds.), Cretaceous Carbonate Platforms, vol. 56. AAPG Mem, pp. 315–324. https://doi.org/10.1306/M56578C25.

Ferrer, O., Roca, E., Benjumea, B., Muñoz, J.A., Ellouz, N., MARCONI Team, 2008. The deep seismic reflection MARCONI-3 profile: role of extensional Mesozoic structure during the Pyrenean contractional deformation at the eastern part of the Bay of Biscay. Mar. Petrol. Geol. 25 (8), 714–730. https://doi.org/10.1016/j.marpetgeo.2008.06.002.

Ferrer, O., Arbués, P., Roca, E., Giles, K.A., Rowan, M.G., De Matteis, M., Muñoz, J.A., 2014. Effect of Diapir Growth on Synkinematic Deepwater Sedimentation: the Bakio

Diapir (Basque-Cantabrian Basin, Northern Spain). American Association of Petroleum Geologists Annual Convention and Exhibition, Houston, USA.
Feuillée, P., Rat, P., 1971. Structures et páleogéographies pyrénéo-cantabriques. In: Debyser, J., Le Pichon, X., Montardet, L. (Eds.), Histoire structurale du Golfe de Gascogne, 2. Ed., 22 Technip, Publications de l'Institut Française du Pétrole, Collection Colloques et Séminaires, pp. 1–48.
Floquet, M., 2004. 3.5.10 el Cretácico superior de la Cuenca Vasco-Cantábrica y áreas adyacentes. In: Vera, J.A. (Ed.), Geología de España. SGE-IGME, Madrid, pp. 299–306.
Frankovic, A., 2011. Análisis cinemático de la pared de sal Euskal Balea (Golfo de Vizcaya) y de los diapiros salinos de Salinas de Añana y Maestu (Cuenca Vasco-Cantábrica, Álava). Ph.D. thesis. UPV-EHU, Getxo, Spain. http://hdl.handle.net/10810/12223.
Frankovic, A., Eguiluz, L., Martínez-Torres, L.M., 2016. Geodynamic evolution of the salinas de Añana diapir in the Basque-Cantabrian Basin, western Pyrenees. J. Struct. Geol. 83, 13–27. https://doi.org/10.1016/j.jsg.2015.12.001.
García-Mondéjar, J., 1982. Tectónica sinsedimentaria en el Aptiense y Albiense de la Región Vasco-Cantábrica Oriental. Cuad. Geol. Iber. 8, 23–36.
García-Mondéjar, J., 1987. Aptian-Albian carbonate episode of Basque-Cantabrian Basin, northern Spain. AAPG Bull. 71, 558. https://doi.org/10.1002/9781444303834.ch10.
García-Mondéjar, J., 1989. Strike-slip subsidence of the Basque-Cantabrian basin of the northern Spain and its relationship to Aptian-Albian opening of Bay of Biscay. In: Tankard, A.J., Balkwill, H.R. (Eds.), Extensional Tectonics and Stratigraphy of the North Atlantic Margins, vol. 46. AAPG Mem, pp. 395–410.
García-Mondéjar, J., García-Pascual, I., 1982. Estudio geológico del anticlinorio de Bilbao entre los ríos Nervión y Cadagua. Kobie 12, 101–137.
García-Mondéjar, J., Robador, A., 1987. Sedimentación y paleogeografía del Complejo Urgoniano (Aptiense-Albiense) en el área de Bermeo (región Vasco-Cantábrica septentrional). Acta Geol. Hisp. 21–22, 411–418.
García-Mondéjar, J., Agirrezabala, L.M., Aramburu, A., Fernández-Mendiola, P.A., Gómez-Pérez, I., López-Horgue, M.A., Rosales, I., 1996. The Aptian-Albian tectonic pattern of the Basque-Cantabrian Basin (northern Spain). Geol. J. 31, 13–45. https://doi.org/10.1002/(SICI)1099-1034 (199603)31:1<13::AID-GJ689>3.0.CO;2-Y.
García-Mondejar, J., Fernández-Mendiola, P.A., Agirrezabala, L.M., Aramburu, A., López-Horgue, M.A., Iriarte, E., Martínez de Rituerto, S., 2004. 3.5.8 el Aptiense-Albiense de la Cuenca Vasco-Cantábrica. In: Vera, J.A. (Ed.), Geología de España. SGE-IGME, Madrid, pp. 291–296.
García-Mondejar, J., López-Horgue, M.A., Aramburu, A., Fernández-Mendiola, P.A., 2005. Pulsating subsidence during a rift episode: stratigraphic and tectonic consequences (Aptian-Albian, northern Spain). Terra. Nova 17 (6), 517–525. https://doi.org/10.1111/j.1365-3121.2005.00644.x.
García-Senz, J., Rosales, J., Robador, A., Pedrera, A., 2019. 5.2.1 the Basque-Cantabrian rift basin. In: Quesada, C., Oliveira, J.T. (Eds.), The Geology of Iberia: A Geodynamic Approach. Volume 3: the Alpine Cycle. Springer Natura Switzerland, Cham, pp. 171–182.
Gariel, O., Bois, C., Curnelle, R., Lefort, J.P., Rolet, J., 1997. The ECORS Bay of Biscay deep seismic survey. Geological framework and overall presentation of the work. Mem. Soc. Geol. Fr. 171, 7–19.
Giles, K.A., Lawton, T.F., 2002. Halokinetic sequence stratigraphy adjacent to the El Papalote diapir, northeastern Mexico. AAPG Bull. 86, 823–840.
Giles, K.A., Lawton, T.F., Rowan, M.G., 2004. Summary of halokinetic sequence characteristics from outcrop studies of La Popa salt basin, northeastern Mexico. In: Post, P.J., Olson, D.L., Lyons, K.T., Palmes, S.L., Harrison, P.F., Rosen, N.C. (Eds.), Salt-sediment Interactions and Hydrocarbon Prospectivity: Concepts, Applications, and Case Studies for the 21st Century. Society of Economic Paleontologists and Mineralogists Gulf Coast Section, 24th annual research conference, pp. 1045–1062.
Giles, K.A., Druke, D.C., Mercer, D.W., Hunnicutt-Mack, L., 2008. Controls on Upper Cretaceous (Maastrichtian) herorozoan carbonate platforms developed on salt diapirs, La Popa Basin, NE Mexico. In: Lukasik, J., Simo, J.A. (Eds.), Controls on Carbonate Platform and Reef Development, vol. 89. SEPM Spec. Pub., pp. 107–124. https://doi.org/10.2110/pec.08.89.0107
Giles, K.A., Rowan, M.G., 2012. Concepts in halokinetic-sequence deformation and stratigraphy. In: Archer, S.G., Alsop, G.I., Hartley, A.J., Grant, N.T., Hodgkinson, R. (Eds.), Salt Tectonics, Sediments and Prospectivity, vol. 363. Geol. Soc. London, Spec. Publ., pp. 7–31
Giles, K.A., Rowan, M.G., Langford, R., McFarland, J., Hearon, T., 2018. Salt shoulders. In: AAPG Search and Discovery. AAPG International Conference and Exhibition, London, England.
Gómez, M., Vergés, J., Riaza, C., 2002. Inversion tectonics of the northern margin of the Basque Cantabrian Basin. Bull. Soc. Geol. Fr. 173 (5), 449–460.
Granado, P., Roca, E., Strauss, Ph, Pelz, K., Muñoz, J.A., 2018. Structural styles in fold-and-thrust belts involving early salt structures: the Northern Calcareous Alps (Austria). Geology 47 (1), 51–54. https://doi.org/10.1130/G45281.1.
Grant, R.J., Underhill, J.R., Hernández-Casado, J., Baker, S.M., Jamiezon, R.J., 2019. Upper Permian Zechstein supergroup carbonate–evaporite platform palaeomorphology in the UK southern North Sea. Mar. Petrol. Geol. 100, 484–518. https://doi.org/10.1016/j.marpetgeo.2017.11.029.
Haq, B.U., 2014. Cretaceous eustasy revisited. Global Planet. Change 113, 44–58.
Hattori, K.E., Loucks, R.G., Kerans, C., 2019. Stratal architecture of a halokinetically controlled patch reef complex and implications for reservoir quality: a case study from the Aptian James Limestone in the Fairway Field, East Texas Basin. Sediment. Geol. 387 (1), 87–103.
Hearon, T.E., Rowan, M.G., Giles, K.A., Hart, W.H., 2014. Halokinetic deformation adjacent to the deepwater Auger diapir, Garden Banks 470, northern Gulf of Mexico: testing the applicability of an outcrop-based model using subsurface data. Interpretation 2, SM57–SM76.
Hearon, T.E., Rowan, M.G., Kernen, R.A., Giles, K.A., Gannaway, C.E., Lawton, T.F., Fiduk, J.C., 2015. Allochthonous salt initiation and advance in the Flinders and Willouran ranges, South Australia: using outcrops to test subsurface-based models from the northern Gulf of Mexico. AAPG Bull. 99 (2), 293–331. https://doi.org/10.1306/08111414022.
Hempel, V.P.M., 1967. Der diapir von Poza de la Sal (Nordspanien). Beih. Geol. Jb. Hannover 66, 95–126.
Hudec, M.R., Jackson, M.P.A., 2007. Terra infirma. Understanding salt tectonics. Earth Sci. Rev. 82, 1–28. https://doi.org/10.1016/j.earscirev.2007.01.001.
Hudec, M.R., Jackson, M.P.A., Schultz-Ela, D.D., 2009. The paradox of minibasin subsidence into salt: clues to the evolution of crustal basins. Geol. Soc. Am. Bull. 121, 201–221.
Jackson, M.P.A., Hudec, M.R., 2017. Salt tectonics. In: Principles and Practice. Cambridge University Press, Cambridge, p. 498.
Jammes, S., Manatschal, G., Lavier, L., Masini, E., 2009. Tectonosedimentary evolution related to extreme crustal thinning ahead of a propagating ocean: example of the western Pyrenees. Tectonics 28 (4). https://doi.org/10.1029/2008TC002406.
Jammes, S., Manatschal, G., Lavier, L., 2010. Interaction between prerift salt and detachment faulting in hyperextended rift systems: the example of the Parentis and Mauléonbasins (Bay of Biscay and western Pyrenees). AAPG Bull. 94, 957–975.
Johnson, H.A., Bredeson, D.H., 1971. Structural development of some shallow salt domes in Louisiana Miocene productive belt. AAPG Bull. 55, 204–226.
Kane, K.E., Jackson, C.A., Larsen, E., 2010. Normal fault growth and fault-related folding in a salt influenced rift basin: south Viking Graben, offshore Norway. J. Struct. Geol. 32 (4), 4980, 506.
Kergaravat, C., Ribes, C., Callot, J.P., Ringenbach, J.C., 2017. Tectono-stratigraphic evolution of salt-controlled minibasins in a fold and thrust belt, the Oligo-Miocene central Sivas Basin. J. Struct. Geol. 102, 75–97. https://doi.org/10.1016/j.jsg.2017.07.007.
Kernen, R.A., Giles, K.A., Rowan, M.G., Lawton, T.F., Hearon, T.E., 2012. Depositional and halokinetic sequence stratigraphy of the Neoproterozoic Wonoka formation adjacent to Patawarta allochthonous salt sheet, central Flinders ranges, south Australia. In: Archer, S.G., Alsop, G.I., Hartley, A.J., Grant, N.T., Hodgkinson, R. (Eds.), Salt Tectonics, Sediments and Prospectivity, vol. 363. Geol. Soc. London, Spec. Publ., pp. 81–105
Klimowitz, J., Malagón, J., Quesada, S., Serrano, A., 1999. Desarrollo y evolución de estructuras salinas mesozoicas en la parte suroccidental de la Cuenca Vasco-Cantábrica (Norte de España): implicaciones exploratorias. In: Libro Homenaje a José Ramírez del Pozo. Asociación de Geólogos y Geofísicos Españoles del Petroleo (AGGEP), Madrid, pp. 159–166.
Kneller, B., McCaffrey, B., Travis, C.J., Harrison, H., Hudec, M.R., Vendeville, B.C., Peel, F.J., Perkins, B.F., 1995. Modelling effects of salt-induced topography on deposition from turbidity currents. In: Salt, Sediment, and Hydrocarbons. SEPM Gulf Coast Section 16th Annual Research Foundation Conference, pp. 137–145.
Lanaja, J.M., 1987. Contribución de la explotación petrolífera al conocimiento de la geología de España. I.G.M.E, Serv. Publ. Min. Indust. Energ., Madrid.
López-Horgue, M.A., Owen, H.G., Aramburu, A., Fernández-Mendiola, P.A., García-Mondejar, J., 2009. Early late Albian (Cretaceous) of the central region of the Basque-Cantabrian Basin, northern Spain: biostratigraphy based on ammonites and orbitolinids. Cretac. Res. 30, 385–400.
López-Gómez, J., Martín-González, F., Heredia, N., de la Horra, R., Barrenechea, J.F., Cadenas, P., Juncal, M., Diez, J.B., Borruel-Abadia, V., Pedreira, D., García-Sansegundo, J., Farias, P., Galé, C., Lago, M., Ubide, T., Fernández-Viejo, G., Gand, G., 2019. New lithostratigraphy for the Cantabrian Mountains_ A common tectono-stratigraphic evolution for the onset of the Alpine cycle in the W Pyrenean realm, N Spain. Earth Sci. Rev. 188, 249–271. https://doi.org/10.1016/j.earscirev.2018.11.008.
Martín-Chivelet, J., Berástegui, X., Rosales, I., Vilas, L., Vera, J.A., Caus, E., Gräfe, K.U., Mas, R., Puig, C., Segura, M., Robles, S., Floquet, M., Quesada, S., Ruiz-Ortiz, P.A., Fregenal-Martínez, M.A., Salas, R., Arias, C., García, A., Martín-Algarra, A., Meléndez, M.N., Chacón, B., Molina, J.M., Sanz, J.L., Castro, J.M., García-Hernández, M., Carenas, B., García-Hidalgo, J., Gil, J., Ortega, F., 2002. Cretaceous. In: Gibbons, W., Moreno, T. (Eds.), The Geology of Spain. Geological Society of London, London, pp. 255–292.
Martínez-Torres, L.M., 1993. Corte balanceado de la Sierra Cantabria (cabalgamiento de la Cuenca Vasco-Cantábrica sobre la Cuenca del Ebro). Geogaceta 14, 113–115.
Masini, E., Manatschal, G., Tugend, J., Mohn, G., Flament, J.M., 2014. The tectono-sedimentary evolution of a hyper-extended rift basin: the example of the Arzacq-Mauléon rift system (Western Pyrenees, SW France). Int. J. Earth Sci. 103, 1569–1596. https://doi.org/10.1007/s00531-014-1023-8.
Mathey, B., 1987. Les flyschs crétacé supérieur des Pyrénées basques. Mem. Geol. Univ. Dijon 12, 1–399.
Mathieu, C., 1986. Histoire géologique du sous-bassin de Parentis. Bull. Centr. Rech. Expl. Prod. Elf-Aquitaine 10 (1), 22–47.
Mayall, M., Lonergan, L., Bowmn, A., James, S., Milles, K., Primmer, T., Pope, D., Rogers, L., Skeene, R., 2010. The response of turbidite slope channels to growth-induced seabed topography. AAPG (Am. Assoc. Pet. Geol.) Bull. 94, 1011–1030.
McDougall, N.D., Pérez-García, A., Huedo, J.L., Esteban, M., 2009. Stratigraphy, structural framework and sedimentology of the Gaviota limestone formation: gas reservoir in Gaviota field and the Fulmar Permit. Oviedo, Spain. In: Flor, G., et al. (Eds.), Nuevas Contribuciones al Margen Ibérico Atlántico -2009-. 6° Simposio sobre el Margen Ibérico Atlántico MIA09, 1-5 de diciembre de 2009, pp. 105–108.
Mendia, M.S., Gil-Ibarguchi, J.I., 1991. High-grade metamorphic rocks and peridotites along the Leiza fault (western Pyrenees, Spain). Geol. Rundsch. 80, 93–107.

Mianaekere, V., Adam, J., 2020. "Halo-kinematic" sequence-stratigraphic analysis of minibasins in the deepwater contractional province of the Liguro-Provençal basin, Western Mediterranean. Mar. Petrol. Geol. 116, 104307. https://doi.org/10.1016/j.marpetgeo.2020.104307.

Moore, D., Snyder, F.C., Rutkowski, S., 1995. Supra-salt stacked condensed sections (SCS): potential indicators of subsalt stratigraphy. In: Travis, C.J., Harrison, H., Hudec, M.R., Vendeville, B.C., Peel, F.J., Perkins, B.F. (Eds.), Salt, Sediment, and Hydrocarbons. Gulf Coast Section SEPM 16th Annual Research Conference, pp. 195–196.

Moore, C.H., Wade, W.J., 2013. Chapter 2 – the application of the concepts of sequence stratigraphy to carbonate rock sequences. In: Moore, C.H., Wade, W.J. (Eds.), Carbonate Reservoirs: Porosity and Diagenesis in a Sequence Stratigraphic Framework, Developments in Sedimentology, vol. 67, pp. 23–38. https://doi.org/10.1016/B978-0-444-53831-4.00002-1.

Muñoz, J.A., 2002. The Pyrenees. In: Gibbons, W., Moreno, T. (Eds.), The Geology of Spain. Geological Society of London, London, pp. 370–385.

Muñoz, J.A., García-Senz, J., 2010. L'estructura geológica. Talls geològics a través de Catalunya. 1. La Noguera Ribagorçana. In: Atlas Geològic de Catalunya. Institut Cartogràfic i Geològic de Catalunya, Barcelona, pp. 130–131.

Muñoz, J.A., Mencos, J., Roca, E., Carrera, N., Gratacós, O., Ferrer, O., Fernández, O., 2018. The structure of the South-Central-Pyrenean fold and thrust belt as constrained by subsurface data. Geol. Acta 16 (4), 439–460. https://doi.org/10.1344/GeologicaActa2018.16.4.7.

Muñoz, J.A., 2019. Alpine orogeny: deformation and structure in the northern Iberian margin (Pyrenees S.L.). In: Quesada, C., Oliveira, J.T. (Eds.), The Geology of Iberia: A Geodynamic Approach. Volume 3: the Alpine Cycle. Springer Natura Switzerland, Cham, pp. 433–452.

Nelson, C.H., Damuth, J.E., Olson, H.C., 2018. Late Pleistocene bryant canyon turbidite system: implications for Gulf of Mexico minibasin petroleum systems. Interpretation 6 (2), SD89–SD114.

Oluboyo, A.P., Gawthorpe, R.L., Bakke, K., Hadler-Jacobsen, F., 2014. Salt tectonics control on deep-water turbidite depositional settings: Miocene, southwestern Lower Congo Basin, offshore Angola. Basin Res. 26 (4), 597–620. https://doi.org/10.1111/bre.12051.

Pedreira, D., Pulgar, J.A., Gallart, J., Díaz, J., 2003. Seismic evidence of Alpine crustal thickening and wedging from the western Pyrenees to the Cantabrian Mountains (north Iberia). J. Geophys. Res. 108 (B4), 2204. https://doi: 10.1029/2001JB001667.

Pedreira, D., Pulgar, J.A., Gallart, J., Torné, M., 2007. Three-dimensional gravity and magnetic modeling of crustal indentation and wedging in the western Pyrenees-Cantabrian Mountains. J. Geophys. Res. 112, B12405. https://doi.org/10.1029/2007JB005021.

Pedrera, A., García-Senz, J., Ayala, C., Ruiz-Constan, A., Rodríguez-Fernández, L.R., Robador, A., González Menéndez, L., 2017. Reconstruction of the Exhumed Mantle across the North Iberian Margin by crustal-scale 3-D gravity inversion and geological cross section. Tectonics 36 (12), 3155–3177.

Poblet, J., Muñoz, J.A., Travé, A., Serra-Kiel, J., 1998. Quantifying the kinematics of detachment folds using three-dimensional geometry: application to the Mediano anticline (Pyrenees, Spain). Geol. Soc. Am. Bull. 110, 111–125.

Pomar, L., Ward, W.C., 1995. sea-level changes, carbonate production and platform architecture: the Llucmajor platform, Mallorca, Spain. In: Haq, B.U. (Ed.), Sequence Stratigraphy and Depositional Response to Eustatic, Tectonic and Climatic Forcing. Coastal Systems and Continental Margins 1. Springer, Dordrecht, pp. 87–112. https://doi.org/10.1007/978-94-015-8583-5_4.

Poprawski, Y., Basile, C., Agirrezabala, L.M., Jaillard, E., Gaudin, M., Jacquin, T., 2014. Sedimentary and structural record of the Bakio salt diapir (the Basque Country, northern Spain). Basin Res. 26, 746–766.

Poprawski, Y., Christophe, B., Etienne, J., Matthieu, G., Michel, L., 2016. Halokinetic sequences in carbonate systems: an example from the middle Albian Bakio breccias formation (Basque Country, Spain). Sediment. Geol. 334, 34–52. https://doi.org/10.1016/j.sedgeo.2016.01.013.

Prather, B.E., Booth, J.R., Steffens, G.S., Craig, P.A., 1998. Classification, lithologic calibration, and stratigraphic succession of seismic facies of intraslope basins, deep-water Gulf of Mexico. AAPG Bull. 82 (5A), 701–728.

Puelles, P., Ábalos, B., García De Madinabeitia, S., Sánches-Lorda, M.E., Fernández-Armas, S., Gil Ibarguchi, J.I., 2014. Provenance of quartz-rich metamorphic tectonite pebbles from the "Black Flysch" (W Pyrenees, N Spain): an EBSD and detrital zircon LA-ICP-MS study. Tectonophysics 632, 123–137.

Pujalte, V., Robles, S., 2008. Parasecuencias Transgresivo-Regresivas en un Cortejo Transgresivo: parte superior de la Fm Utrillas en Olleros de Pisuerga, Palencia. Geogaceta 44, 187–190.

Quintà, A., Tavani, S., Roca, E., 2012. Fracture pattern analysis as a tool for constraining the interaction between regional and diapir-related stress fields: Poza de la Sal Diapir (Basque Pyrenees, Spain). In: Archer, S.G., Alsop, G.I., Hartley, A.J., Grant, N.T., Hodgkinson, R. (Eds.), Salt Tectonics, Sediments and Prospectivity, vol. 363. Geol. Soc. London, Spec. Publ., pp. 521–532

Quintana, L., 2012. Extensión e Inversion Tectónica en el sector central de la Región Vasco-Cantábrica (Cantabria-Vizcaya, norte de España). Ph.D. thesis, Univ. Oviedo, Oviedo, Spain.

Quintana, L., Pulgar, J.A., Alonso, J.L., 2015. Displacement transfer from borders to interior of a plate: a crustal transect of Iberia. Tectonophysics 663, 1–21.

Rat, P., 1959. Ph.D. thesis. Les Pays Crétacés Basco-Cantabriques (Espagne), 18. Université de Dijon, Dijon, France.

Rat, P., 1988. The Basque-Cantabrian Basin between the Iberian and European plates: some facts but still many problems. Rev. Soc. Geol. Espana 1, 327–348.

Ribes, C., Kergaravat, C., Bonnel, C., Crumeyrolle, P., Callot, J.P., Poisson, A., Temiz, H., Ringenbach, J.C., 2015. Fluvial sedimentation in a salt-controlled mini-basin: stratal patterns and facies assemblages, Sivas Basin, Turkey. Sedimentology 62 (6), 1513–1545. https://doi.org/10.1111/sed.12195.

Ringenbach, J.C., Salel, J.F., Kergaravat, C., Ribes, C., Bonnel, C., Callot, J.P., 2013. Salt tectonics in the Sivas Basin, Turkey: outstanding seismic analogues from outcrops. First Break 31, 57–65.

Robador, A., García-Mondejar, J., 1987. Caracteres sedimentológicos generales del "Flysch-Negro" entre Baquio y Guernica (Albiense superior-Cenomaniense inferior, provincia de Vizcaya). Acta Geol. Hisp. 21–22, 275–282.

Robles, S., Pujalte, V., García-Mondejar, J., 1988. Evolución de los sistemas sedimentarios del Margen continental Cantábrico durante el Albiense y Cenomaniense, en la transversal del litoral vizcaino. Rev. Soc. Geol. Espana 1, 409–441.

Robles, S., Pujalte, V., Vicente, J.C., Quesada, S., 1989. Estratigrafia secuencial del Flysch Negro Vascocantábrico en la transversal de Bilbao, 1989. Volumen XII Congreso Español de Sedimentología, Leioa-Bilbao, pp. 177–186.

Roca, E., Muñoz, J.A., Ferrer, O., Ellouz, N., 2011. The role of the Bay of Biscay Mesozoic extensional structure in the configuration of the Pyrenean orogen: constraints from the MARCONI deep seismic reflection survey. Tectonics 30, TC2001.

Rowan, M.G., 2014. Passive-margin salt basins: hyperextension, evaporite deposition, and salt tectonics. Basin Res. 26, 154–182.

Rowan, M.G., Lindsø, S., 2017. Salt tectonics of the Norwegian Barents Sea and northeast Greenland shelf. In: Soto, J.I., Flinch, J.F., Tari, G. (Eds.), Permo-Triassic Salt Provinces of Europe, North Africa and the Atlantic Margins. Elsevier, Amsterdam, pp. 265–286. https://doi.org/10.1016/B978-0-12-809417-4.00013-6.

Rowan, M.G., Vendeville, B.C., 2006. Foldbelts with early salt withdrawal and diapirism: physical model and examples from the northern Gulf of Mexico and Flinders Ranges, Australia. Mar. Petrol. Geol. 23, 871–891.

Rowan, M.G., Weimer, P.W., 1998. Salt-sediment interaction, northern green canyon and Ewing bank (offshore Louisiana), northern Gulf of Mexico. AAPG Bull. 82, 1055–1082.

Rowan, M.G., Lawton, T.F., Giles, K.A., Ratliff, R.A., 2003. Near-salt deformation in La Popa basin, Mexico, and the northern Gulf of Mexico: a general model for passive diapirism. AAPG Bull. 87, 733–756.

Rowan, M.G., Lawton, T.F., Giles, K.A., 2012a. Anatomy of an exposed vertical salt weld and flanking strata, La Popa Basin, Mexico. In: Archer, S.G., Alsop, G.I., Hartley, A.J., Grant, N.T., Hodgkinson, R. (Eds.), Salt Tectonics, Sediments and Prospectivity, vol. 363. Geol. Soc. London, Spec. Publ, pp. 33–58.

Rowan, M.G., Giles, K.A., Roca, E., Arbués, P., Ferrer, O., 2012b. Analysis of Growth Strata Adjacent to an Exposed Deepwater Salt Diapir, Northern Spain. American Association of Petroleum Geologists Annual Convention, Long Beach, USA.

Rowan, M.G., Giles, K.A., Hearon, T.E., Fiduk, J.C., 2016. Megaflaps adjacent to salt diapirs. AAPG Bull. 100 (11), 1723–1747. https://doi.org/10.1306/05241616009.

Rowan, M.G., Muñoz, J.A., Giles, K.A., Roca, E., Hearon, T.E.I.V., Fiduk, J.C., Ferrer, O., Fischer, M.P., 2020. Folding and fracturing of rocks adjacent to salt diapirs. J. Struct. Geol. (in review).

Ryan, W.B.F., Carbotte, S.M., Coplan, J.O., O'Hara, S., Melkonian, A., Arko, R., Weissel, R.A., Ferrini, V., Goodwillie, A., Nitsche, F., Bonczkowski, J., Zemsky, R., 2009. Global multi-resolution topography synthesis. G-cubed 10 (3). https://doi.org/10.1029/2008GC002332.

Sanchez, F., 1991. Evolución estructural post-kimmérica de la plataforma continental vasco-cantábrica. Ph.D. thesis. Univ. Politécnica de Madrid, Madrid.

Saura, E., Vergés, J., Martín-Martín, J.D., Messager, G., Moragas, M., Razin Grélaud, C., Joussiaume, R., Malaval, M., Homke, S., Hunt, D.W., 2014. Syn- to post-rift diapirism and minibasins of the Central High Atlas (Morocco): the changing face of a mountain belt. J. Geol. Soc. London 171, 97–105.

Saura, E., Vergés, J., Martín-Martín, J.D., Hunt, D.W., 2013. Syn- to post-rift diapirism and minibasins of the Central High Atlas (Morocco): the changing face of a mountain belt. J. Geol. Soc. London 171 (1), 97–105.

Saura, E., Ardèvol, L., Teixell, A., Vergés, J., 2016. Rising and falling diapirs, shifting depocenters, and flap overturning in the Cretaceous Sopeira and Sant Gervàs subbasins (Ribagorça Basin, southern Pyrenees). Tectonics 35, 638–662.

Serrano, A., Martínez del Olmo, W., 1990. Tectónica salina en el Dominio Cántabro-Navarro: evolución, edad y origen de las estructuras salinas. In: Ortí, F., Salvany, J. M. (Eds.), Formaciones evaporíticasde la Cuenca del Ebro y cadenas periféricas y de la zona de Levante. Nuevas aportaciones y guía de superficie. ENRESA e Universitat de Barcelona, Barcelona, pp. 39–53.

Serrano, A., Martínez del Olmo, W., 2004. 3.6.3.1 Estructuras diapíricas en la zona meridional de la Cuenca Vasco-Cantábrica. In: Vera, J.A. (Ed.), Geología de España. SGE-IGME, Madrid, pp. 334–338.

Sibuet, J.C., Srivastava, S.P., Spakman, W., 2004. Pyrenean orogeny and plate kinematics. J. Geophys. Res. 109, B08104. https://doi.org/10.1029/2003JB002514.

Soler, R., José, R., 1972. Las series jurásicas y el "purbeckiense" neocomiense de Guernica. Bol. Geol. Min. 83 (3), 221–230.

Soler, R., López Vilchez, J., Riaza, C., 1981. Petroleum geology of the Bay of Biscay. In: Illing, L.V., Hobson, G.D. (Eds.), Petroleum Geology of the Continental Shelf of North-West Europe. Institute of Petroleum, London, pp. 474–482.

Soto, R., Beamud, E., Roca, E., Carola, E., Almar, Y., 2017. Distinguishing the effect of diapir growth on magnetic fabrics of syn-diapiric overburden rocks: Basque-Cantabrian basin, Northern Spain. Terra. Nova 29, 191–201.

Souquet, P., Peybernés, B., 1991. Stratigraphie séquentielle du cycle Albien dans les Pyrenées franco-espagnoles. Bull. Centr. Rech. Expl. Prod. Elf-Aquitaine 15, 195–213.

Tavani, S., Granado, P., 2014. Along-strike evolution of folding, stretching and breaching of supra-salt strata in the Plataforma Burgalesa extensional forced fold system (northern Spain). Basin Res. 27, 573–585.

Teixell, A., Barnolas, A., Rosales, I., Arboleya, M.L., 2017. Structural and facies architecture of a diapir-related carbonate minibasin (lower and middle Jurassic, High Atlas, Morocco). Mar. Petrol. Geol. 81, 334–360. https://doi.org/10.1016/j.marpetgeo.2017.01.003.

Toniolo, H., Lamb, M., Parker, G., 2006. Depositional turbidity currents in diapiric minibasins on the continental slope: formulation and theory. J. Sediment. Res. 76 (5), 783–797.

Tugend, J., Manatschal, G., Kusznir, N.J., Masini, E., Mohn, G., Thinon, I., 2014. Formation and deformation of hyperextended rift systems: insights from rift domain mapping in the Bay of Biscay-Pyrenees. Tectonics 33, 1239–1276. https://doi.org/10.1002/2014TC003529.

Vendeville, B., Jackson, M.P.A., 1992. The rise of diapirs during thin-skinned extensión. Mar. Petrol. Geol. 9, 331–353.

Vergés, J., Moragas, M., Martín-Martín, J.D., Saura, E., Casciello, E., Razin, P.H., Grelaud, G., Malaval, M., Joussiaume, R., Messager, G., Sharp, I., Hunt, D.W., 2017. Chapter 26 – salt tectonics in the Atlas Mountains of Morocco. In: Soto, J.I., Flinch, J. F., Tari, G. (Eds.), Permo-Triassic Salt Provinces of Europe, North Africa and the Atlantic Margins. Tectonics and Hydrocarbon Potential. Elsevier, Amsterdam, pp. 563–579.

Vicente-Bravo, J.C., Robles, S., 1991a. Geometría y modelo deposicional de la secuencia Sollube del Flysch Negro (Albiense medio, norte de Bizkaia). Geogaceta 10, 69–72.

Vicente-Bravo, J.C., Robles, S., 1991b. Caracterización de las facies de transición canal-lóbulo en la secuencia de Jata del Flysch Negro (Albiense Superior, norte de Vizcaya). Geogaceta 10, 72, 72.

Voort, H.B., 1964. Zum Flyschproblem in den Westpyrenäen. Geol. Rundsch. 53, 220–233.

Warren, J., 2006. Evaporites: Sediments, Resources, and Hydrocarbons. Springer Berlin, p. 1035.

Wiedmann, J., Reitner, J., Engeser, T., Schwentke, W., 1983. Plattentektonik, Fazies- und Subsidenzgeschichte des basko-kantabrischen Kontinentalrandes wahrend Kreide und Alttertitir. Zitteliana 10, 207–244.

Wilson, P., Elliot, G.M., Gawthorpe, R.L., Jackson, C.A., Michelsen, L., Sharp, I.R., 2013. Geometry and segmentation of an evaporite-detached normal fault array: 3D seismic analysis of the southern Bremstein Fault Complex, offshore mid-Norway. J. Struct. Geol. 51, 74–91.